

Method for Indirect Validation of Ozone Mapping Profiler Suite (OMPS) Limb

Retrievals Using the RAQMS-Aura Reanalysis, ozonesondes, and ACE-FTS

by

Margaret Bruckner

A thesis submitted in partial fulfillment of

the requirements for the degree of

MASTERS OF SCIENCE

(Atmospheric and Oceanic Sciences)

At the

UNIVERSITY OF WISCONSIN-MADISON

2020

Abstract

The onset of stratospheric ozone recovery is projected to become apparent between 2017 and 2021. Alongside this onset, there is turnover occurring in the satellite instrumentation which measures ozone, with current generation instruments such as the NASA Ozone Monitoring Instrument (OMI) and Microwave Limb Sounder (MLS) being replaced by next generation instrumentation such as the Ozone Mapping Profiler Suite (OMPS). Chemical re-analyses have been developed using OMI and MLS retrievals, as well as using other satellite retrievals of atmospheric constituents. For continued use in investigation of ozone interannual variability and trends associated with ozone recovery, the re-analyses must be able to assimilate OMPS limb and nadir retrievals. To assimilate this data into re-analyses such as the Real-time Air Quality Modeling System (RAQMS), a good estimate of the bias for OMPS limb is needed to assess the impact of assimilating OMPS limb measurements on the re-analysis. This study develops the framework for carrying out an indirect validation of OMPS limb UV and visible retrievals utilizing the RAQMS Aura reanalysis, selected ozonesondes, and Atmospheric Chemistry Experiment Fourier transform spectrometer (ACE-FTS) ozone retrievals.

Acknowledgements

There are many people without whom this thesis would not have been possible. First, my undergraduate advisor Dr. Steve Kolmes. I may not have needed much assistance in choosing courses or ensuring I met graduation requirements, but your encouragement to take courses I found interesting and guidance through the grad school application and acceptance process were invaluable. Next, to my advisor here at UW-Madison Dr Brad Pierce. While there is a great deal more to thank you for, here I express my gratitude to you for taking me on as your graduate student and aiding me in focusing the directions of this research. To the other members of my masters committee, Drs. Jack Fishman and Matthew Hichman, thank you for the comments you provided on multiple drafts of this thesis. Without the feedback you provided the scientific story presented in this thesis would be incomplete. Additional thanks to those friends I've met during my time in Madison- both in the department and through Ultimate Frisbee. The drinks, conversation, and other non-research activities have been essential for keeping me sane and developing a work-life balance.

Finally, to my family without whose love and support throughout my entire life I wouldn't have been able to accomplish anything. You can quit asking if I finished my masters now.

Table of Contents	
Abstract	i
Acknowledgements	ii
Table of Contents	iii
List of Figures and Tables	v
List of Acronyms	vii
1. Introduction	1
2. Background	3
2.1 Stratospheric Ozone.....	3
2.2 Satellite Observing Systems	5
2.3 Overview of Validation Methods	8
2.4 Chemical Re-analyses	9
3. Data	12
3.1 ACE-FTS.....	12
3.2 Ozonesondes.....	14
3.3 OMPS	16
3.4 RAQMS Aura Reanalysis.....	17
4. Method and Results	18
4.1 Overview of non-coincident OMPS validation	18
4.2 ACE-FTS Analysis and Bias Correction of RAQMS-Aura	18
4.2.1 Removal of Physically Unrealistic Outliers from ACE-FTS	19
4.2.2 Bias in RAQMS-Aura relative to ACE-FTS Sunrise Retrievals	20
4.2.3 Bias in RAQMS-Aura relative to ACE-FTS Sunset Retrievals	25
4.2.4 RAQMS-Aura Bias Correction	28
4.3 Ozonesondes.....	30
4.3.1 ESRL ozonesondes	33
4.3.2 SHADOZ Ozonesondes.....	37
4.3.3 Summary of Ozonesonde analysis.....	41
4.4 OMPS-L Validation	41
4.4.1 Visible Retrieval.....	42
4.4.2 UV Retrieval.....	44
4.4.3 Overlap of UV and Visible Retrievals.....	46

4.4.4 Seasonal Cycle in combined retrieval	47
5. Conclusion.....	50
6. References	52

List of Figures and Tables

Table 1. Ozonesonde station locations, data providers, and years available during 2006-2016.....	15
Table 2. Pearson Correlation between ozonesondes and coincident RAQMS Aura simulated Ozone mixing ratio.....	32
Figure 1. ACE-FTS Annual Sampling by month for SS and SR retrievals. The number of samples is not an annual average, as all latitudes at which an observation was made between January 1, 2006 and December 31, 2016 are plotted.	13
Figure 2. ACE-FTS SR and RAQMS-Aura Zonal Median ozone concentration in ppmv.	22
Figure 3. Difference in ppmv between ACE-FTS retrieval median and RAQMS Aura median for the entire 2006-2016 time period.	23
Figure 4. Median absolute deviation in ppmv for ACE-FTS SR and coincident RAQMS-Aura.....	24
Figure 5. ACE-FTS SS and RAQMS-Aura Zonal Median ozone concentrations in ppmv.	26
Figure 6. Median absolute deviation in ppmv for ACE-FTS SS and coincident RAQMS-Aura.....	27
Figure 7. Bias Correction for RAQMS-Aura. Derived from median ACE-FTS SS and SR difference with coincident RAQMS-Aura.....	29
Figure 8. Scatter plots showing (left) the relationship between ozonesonde measurements and corrected RAQMS Aura values and (right) magnitude of the correction as percentage of the ozonesonde value.....	33
Figure 9. Average percent bias between all ESRL ozonesonde profiles and coincident RAQMS-Aura profiles.....	36
Figure 10. Bias, expressed in percent, between RAQMS-Aura and SHADOZ ozonesonde measurements. SHADOZ sites at Natal Brazil, Nairobi Kenya, and Kuala Lumpur Malaysia were used.....	39

Figure 11. Profile of percent bias of RAQMS-Aura to SHADOZ ozonesonde measurements, expressed as a function of altitude from tropopause. SHADOZ sites at Natal Brazil, Nairobi Kenya, and Kuala Lumpur Malaysia.....	40
Figure 12. Difference in mean and standard deviation between OMPS-L visible retrievals and RAQMS-Aura.	44
Figure 13. Regionally binned percent bias in OMPS-L visible retrievals for a) 90°-60° S; b) 60°-20° S; c) 20° S-20° N; d) 20°-60° N; e) 60°-90° N.	44
Figure 14. Differences for a) mean and b) standard deviation between OMPS-L UV retrievals and RAQMS-Aura retrievals.	45
Figure 15. Regionally binned percent bias in OMPS-L UV retrievals for a) 90°-60° S; b) 60°-20° S; c) 20° S-20° N; d) 20°-60° N; e) 60°-90° N.	45
Figure 16. Percent difference between OMPS-L UV and visible retrievals at retrieval overlap altitudes of 30.5 km, 31.5 km, 32.5 km, 33.5 km, 34.5 km, and 35.5 km.	46
Figure 17. Average seasonal cycle at 65°-70°N, expressed a as percent deviation from the mean for OMPS in ppmv.	48
Figure 18. As in Fig. 17, except for the latitude band 25°-30°S.....	49
Figure 19. As in Fig. 17, except for the latitude band 50°-55°S.....	49
Figure 20. Seasonal cycle expressed as a percent deviation from mean for OMPS, and calculated from number density.....	49

List of Acronyms

- AATSR: Advanced Along-Track Scanning Radiometer
- ACE-FTS: Atmospheric Chemistry Experiment Fourier Transform Spectrometer
- AIRS: atmospheric infrared sounder
- AOD: Aerosol Optical Depth
- CAMS: Copernicus Atmosphere Monitoring Service
- CFC: Chlorofluorocarbon
- ECC: electrochemical concentration cell
- ESRL-GMD: Earth System Research Laboratory Global Monitoring Division
- ESA: European Space Agency
- GEOS-5: Goddard Earth Observing System Model, Version 5
- GOME: Global Ozone Monitoring Experiment
- GSI: Grid-point Statistical Interpolation
- JRAero: Japanese Reanalysis for Aerosol
- MAD: Median average deviation
- MAESTRO: Measurement of Aerosol Extinction in the Stratosphere and Troposphere Retrieved by Occultation
- MeAD: mean absolute deviation about the median
- MERRA-2: Modern-Era Retrospective analysis for Research and Applications, Version 2
- MIPAS: Michelson interferometer for passive atmospheric sounding
- MLS: Microwave Limb Sounder
- MODIS: moderate resolution imaging spectrometer
- MOPITT: Measurement of Pollution in the Troposphere
- ODS: Ozone Depleting Substance
- OMI: Ozone Monitoring Instrument
- OMPS: Ozone Mapping Profiler Suite
- OMPS-L: Ozone Mapping Profiler Suite Limb Sounder

OMPS-N: Ozone Mapping Profiler Suite Nadir Profiler

RAQMS: Real-time Air Quality Modeling System

SAGE: Stratospheric Aerosol and Gas Experiment

SAM: Stratospheric aerosol measurement

SBUV: Solar Backscatter Ultraviolet

SCIAMACHY: Scanning Imaging Absorption Spectrometer for Atmospheric Chemistry

SHADOZ: Southern Hemisphere Additional Ozonesondes

S-NPP: Suomi National Polar-orbiting Partnership

TOMS: Total Ozone Mapping Spectrometer

UARS: Upper Atmosphere Research Satellite

UTLS: Upper Troposphere/Lower Stratosphere

WMO: World Meteorological Organization

WOUDC: World Ozone and Ultraviolet Radiation Data Centre

1. Introduction

Ozone is an important atmospheric trace gas for several reasons, including its role in absorption of ultra-violet (UV) radiation and in climate regulation (World Meteorological Organization, 1995). In the troposphere, ozone is an atmospheric pollutant formed in photochemical oxidation reactions of nitrogen oxides, carbon monoxide, and volatile organic compounds (Crutzen, 1988; Monks et al., 2015). Forecasts and analyses of global tropospheric and stratospheric ozone concentrations can provide estimates of the distribution of ozone in the atmosphere. Chemical re-analyses are becoming available and are a useful tool for investigation of trends in atmospheric ozone concentrations (Bai, Chang, Shi, Yu, & Gao, 2017; Wargan et al., 2017). Re-analyses are reliant on input of well-validated satellite records with well-characterized errors and uncertainties. Validation of satellite data requires independent datasets and can be done directly (eg. Dupuy et al., 2009) or indirectly (eg. Considine et al., 2008). A direct validation requires observations that are paired in space and time while indirect validations use alternative methods to infer the degree of bias inherent to the measurement. The difference between the two types of validation are described in greater detail in chapter 2 of this thesis. Indirect validation provides a more statistically robust approach than a direct validation through inclusion of increased number of data points (Considine et al., 2008; Lait et al., 2004). This study calculates Ozone Mapping Profiler Suite Limb profiler (OMPS-L, (Flynn, Hornstein, & Hilsenrath, 2004)) ozone mean and seasonal biases through indirect validation of OMPS-L with ozonesonde and Atmospheric Chemistry Experiment Fourier Transform Spectrometer (ACE-FTS, (Bernath et al., 2005)) data through use of the Real-time Air Quality Modeling System

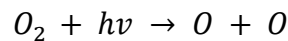
(RAQMS, (Pierce et al., 2007)) Aura reanalysis as a transfer standard. The outcomes of this study are: 1) the development of a framework for evaluating bias in atmospheric chemical concentration measurements using RAQMS-Aura; and 2) a specific calculation of OMPS-L ozone profile biases for use in data assimilation.

This thesis is organized as follows. Chapter 2 will provide an overview of ozone chemistry, satellite ozone retrievals, chemical reanalysis, and validation techniques. Chapter 3 outlines the characteristics of ACE-FTS, ozonesondes, OMPS-L and RAQMS-Aura. The method for data analysis and discussion of the results are presented in chapter 4. A summary of the study and implications on assimilation of OMPS-L into RAQMS are discussed in chapter 5.

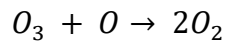
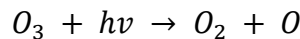
2. Background

2.1 Stratospheric Ozone

The distribution of ozone in the atmosphere results from the combined influence of radiation, dynamics, and chemistry (Holton et al., 1995). The Chapman mechanism was initially proposed by Sidney Chapman in 1930 to explain the distribution of stratospheric ozone and its annual variation through oxygen-only chemistry initialized by UV radiation (Chapman, 1930). It encompasses a series of 5 oxygen-only reactions where high energy photons in the UV portion of the radiation spectrum break apart bonds between oxygen atoms to initiate both the formation and destruction reaction sequences. The ozone formation sequence of reactions is:

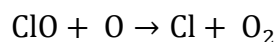
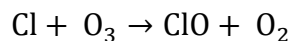


The ozone destruction sequence of reactions is:



M is used to represent a nonreactive participant in the reaction that is present to act either as a catalyst or absorb excess energy from the reaction. Ozone concentration reaches a peak in the middle stratosphere (near 30 km), in terms of ozone mixing ratio, and in the lower stratosphere (near 21 km), in terms of ozone concentration. This height is the result of the presence of sufficient oxygen density and the level of penetration of solar UV radiation into the atmosphere (Fishman, 2003).

The Chapman mechanism is insufficient to fully describe the distribution and concentration in Earth's atmosphere given its neglect of transport and exclusion of catalytic cycles involving species such as hydroxyl radicals and nitrogen oxides. It is estimated that considering only the Chapman mechanism overestimates atmospheric ozone concentrations by at least double (Jacob, 1999). The influence of catalytic cycles on stratospheric ozone concentration can be seen most dramatically above Antarctica during the spring in the southern hemisphere, where the isolation of air by the polar vortex and formation of chlorine oxides on the surface of polar stratospheric clouds enhances ozone loss and results in the "ozone hole" (Solomon, 1999). A catalytic cycle is a series of chemical reactions where a catalyst is required for reactions to occur but does not factor into the net reaction for the cycle. A sample catalytic cycle involving chlorine is represented by the sequence:



Other catalytic cycles resulting in net ozone depletion involve chemical species containing hydroxyl, nitrogen, chlorine, or bromine (Solomon, 1999). Chlorofluorocarbons (CFCs) are an anthropogenic compound that has been identified as a major source of chlorine for catalytic ozone destruction (Molina & Rowland, 1974; Stolarski & Cicerone, 1974). The implementation of the Montreal Protocol and its amendments seeks to reverse the trend in enhanced seasonal depletion of ozone through policies outlawing use of CFCs and eventually its less destructive replacement compounds (WMO, 2018).

Following the passage and implementation of the Montreal Protocol, the amount of ozone depleting substances (ODS) in the stratosphere has declined (Hassler et al., 2011). The impact of this decline on stratospheric ozone concentrations may be inferred through use of a variety of statistical methods of calculating trends. A weakly positive trend in upper stratospheric ozone in global merged satellite ozone records since 1997 can be calculated (Sofieva et al., 2017; Steinbrecht et al., 2017) using statistical methods such as multivariate regression on ozone anomalies. The multivariate regressions account for solar cycle, the quasi-biennial oscillation, and the El Niño-Southern Oscillation (Sofieva et al., 2017; Steinbrecht et al., 2017). This positive trend is statistically significant in the extratropical upper stratosphere (Sofieva et al., 2017).

Beyond the statistically significant trend, other signs of ozone recovery have been noted (e.g. de Laat et al., 2017; Ziemke & Chandra, 2012; Solomon et al., 2016). The average daily ozone mass deficit for the Antarctic shows a statistically significant decrease between 2001 and 2015, and is highly correlated with equivalent effective stratospheric chlorine, an ODS proxy measurement (de Laat et al., 2017). South Pole loss rates are expected to first become significantly lower than they were at the peak loss period around 2017-2021 (Hassler et al., 2011). Stratospheric ozone concentrations are predicted to recover to mid-1980s concentrations post 2020 (Ziemke & Chandra, 2012).

2.2 Satellite Observing Systems

Satellite observations of ozone were made in 1970 with the Backscatter Ultraviolet (BUV) experiment onboard Nimbus-4 (Donald F. Heath, Mateer, & Krueger, 1973). Following the initial experiment, satellite observations of ozone have been made continuously since 1978 beginning with the Total Ozone Mapping Spectrometer (TOMS)

and Solar Backscatter Ultraviolet (SBUV) series of instruments onboard the polar-orbiting Nimbus satellites (Frederick, Cebula, & Heath, 1986; D. F. Heath, Krueger, Roeder, & Henderson, 1975; Hilsenrath et al., 1995; McPeters, Bhartia, Haffner, Labow, & Flynn, 2013). These instruments measured ultraviolet radiation to obtain total column and profile ozone measurements. The TOMS dataset has a higher temporal and horizontal resolution than SBUV, although is coarse in comparison to that of more recent instrumentation. Measurements of total column ozone have also been made with the European Space Agency (ESA) Global Ozone Monitoring Experiment (GOME) (Burrows et al., 1999), the ESA's Scanning Imaging Absorption Spectrometer for Atmospheric Chartography (SCIAMACHY) (Bovensmann et al., 1999), and NASA's Ozone Monitoring Instrument (OMI) (Levelt et al., 2006).

Solar occultation ozone measurements are made using a photometer to measure direct transmission of sunlight through the atmospheric limb at sunrise and sunset. There have been many satellites collecting ozone measurements by solar occultation. Some of these include the Stratospheric Aerosol and Gas Experiment (SAGE) series of instruments and the Atmospheric Chemistry Experiment Fourier Transform Spectrometer (ACE-FTS). While temporal and horizontal resolution of these measurements are low, they generally have high vertical resolution and high precision (Bernath 2016; McCormick et al., 1989).

The first microwave limb sounding observations of ozone from satellite were made in 1991 with a microwave limb sounder (MLS) on the Upper Atmosphere Research Satellite (UARS) (Waters et al., 1998). The UARS MLS ozone retrieval had a vertical

range of approximately 15 km to 80 km, and average accuracy of ~3% (Waters et al., 1999). The UARS MLS took daily measurements until 1994, and then limited measurements until August 2001. The follow-on instrument to the UARS MLS came online in 2004 as the MLS on the Earth Observing System Aura satellite (Waters et al., 2006). The scanning and calibration occur at a faster time interval on the Aura MLS. The Aura MLS also has additional channels, which are used to obtain measurements of additional atmospheric constituents (Waters et al., 2006).

The launch of Suomi National Polar-orbiting Partnership (S-NPP) in October 2011 marks a shift to the next generation of satellites and sensors, with replacement of OMI, MLS, and solar backscatter ultraviolet radiometer-2 (SBUV/2) instruments by the Ozone Mapping Profiler Suite (OMPS) package. OMPS consists of two instruments providing ozone measurements- the limb sounder (OMPS-L) and the nadir profiler (OMPS-N). OMPS-N is the next generation sensor replacement for OMI and SBUV/2 (Flynn, Hornstein, & Hilsenrath, 2004). OMPS-L is a research instrument providing continuous daytime profile measurements in the UV and visible portions of the spectrum, returning separate UV and visible retrievals. The full OMPS instrument package was included on S-NPP, while only the OMPS-N instrument was included onboard NOAA-20 which launched on November 18, 2017. Both OMPS-N and OMPS-L are scheduled for inclusion onboard the next three satellites in the series, referred to pre-launch as JPSS-2, JPSS-3, and JPSS-4.

2.3 Overview of Validation Methods

Satellite validation is the practice of comparing observations from a satellite with an independent reference truth value to calculate the accuracy of the observation (Loew et al., 2017). The reference truth value is in practice taken as an independent observation or analysis of the same variable. An unbiased truth value is unobtainable, as all observations and calculated analyses are known to be biased in some way. Traditional approaches to satellite validation require near-coincidence between two observations, where a single well-validated observing system or a series of observing systems serves as the comparison or truth observation (eg. Dupuy et al., 2009; Froidevaux et al., 2008). Coincidence criteria are used to select measurements obtained within a set period and geographic distance of another measurement.

While direct comparison of two observations is a very good way to determine how correct a measurement is, this method limits the strength of the bias determination by throwing out otherwise valid measurements due simply to the fact that they are not within what has been defined as reasonably close to another measurement. The constraints of coincidence result in a greatly reduced number of observations on which to calculate statistics. This may skew statistics in several ways. The sampled observations may not be representative of the full distribution, thereby resulting in mean and spread statistics that are not accurate for all observations. There may also not be enough observations from which to obtain robust statistics. For example, an instrument with high precision and low sampling frequency such as solar occultation makes up to 30 measurements a day while a typical backscatter instrument makes orders of magnitude more measurements a day. The direct comparison of the two would be able to use at most

30 points of the high frequency satellite observations. Such a comparison would not be very robust due to a small sample size. The statistics also show a spatial weighting, as some latitude and longitude pairs are observed while others are not.

Non-coincident techniques alleviate some of these problems by use of an intermediate between sets of observations or mapping of measurements to alternate coordinate systems, increasing the number of observations included in the statistics as the necessity of a direct coincidence is lessened. Measurements may be mapped to an alternate coordinate system such as the time-invariant potential vorticity (PV) – potential temperature (θ) space and then grouped based on the new coordinate system (Lait et al., 2004). There are several methods that may generally be summarized as evolving measurements forward or backward in time and space to the time and location of another measurement (eg. Danilin et al., 2002; Morris et al., 2002; Considine et al., 2008). Another form of non-coincident validation is the use of an intermediate dataset such as model analyses to compare sets of non-coincident measurements against (eg. Kopacz et al. 2010; Zhang et al., 2010). This method is still limited by the sampling patterns of instruments but does increase the number of observations from both datasets that may be included to all valid observations.

2.4 Chemical Re-analyses

Additional observations may be included in a validation of OMPS-L through use of a non-coincident validation technique where a re-analysis with an ozone field is used as the intermediary between the comparison measurement and the OMPS-L retrievals. An analysis is an estimate of the state of the atmosphere at a given instance in time where forecasts and observations are combined in a statistically consistent way that takes into

account observation and forecast errors (“Analysis - AMS Glossary,” n.d.). There are two categories under which re-analyses containing an ozone variable fall: meteorological re-analyses in which there is limited chemical information and chemical re-analyses where satellite measurements are used to constrain a large suite of chemical species. An example of a meteorological re-analysis would be the Modern-Era Retrospective analysis for Research and Applications, Version 2 (MERRA-2) re-analysis (Bosilovich et al., 2015), which utilizes the NASA Goddard Earth Observing System Model, Version 5 (GEOS-5), and contains ozone and aerosol fields. The MERRA-2 ozone and aerosol fields are constrained with MLS ozone profiles, SBUV ozone, OMI total column ozone, and AVHRR, MODIS, MISR, and AERONET AOD (McCarty et al., 2015; Randles et al., 2017). Two existing chemical re-analyses are Japanese Reanalysis for Aerosol (JRAero) (Yumimoto et al., 2017) and the Copernicus Atmosphere Monitoring Service (CAMS) reanalysis (Inness et al., 2019). The CAMS reanalysis assimilates SCIMACHY, OMI, and GOME-2 total column ozone, Michelson interferometer for passive atmospheric sounding (MIPAS) and MLS ozone profile, SBUV/2 partial ozone column, Measurement of Pollution in the Troposphere (MOPITT) total column CO, SCIMACHY, OMI, and GOME-2 tropospheric NO₂ column, and moderate resolution imaging spectrometer (MODIS) and Advanced Along-Track Scanning Radiometer (AATSR) AOD using an incremental 4D-Var data assimilation system (Inness et al., 2019). The JRAero version 1.0 reanalysis assimilates MODIS AOD using a 2-d variational data assimilation system (Yumimoto et al., 2017).

Reanalysis datasets provide several advantages over purely satellite datasets. Reanalyses are more consistent and regular in time and space, presenting a look at global distributions every model output time, whereas a polar orbiting satellite in sun-synchronous orbit might obtain global coverage every few days. In a validation study, the consistent time resolution and global gridded variables allow for finding a near-coincidence for every observation. The increased temporal resolution of a reanalysis allows for better investigation of time dependent trends, as it will increase the probability that the model captures short time scale variation- such as diurnal and other sub-seasonal variability. Satellite datasets also generally do not contain detailed chemical information, and so the addition of this in models allows for increased study of the chemistry associated with trends and phenomena in ozone concentration.

3. Data

This study uses three independent datasets to validate OMPS limb ozone. These independent datasets are: 1) Atmospheric Chemistry Experiment Fourier Transform Spectrometer ozone profile retrievals; 2) NOAA Earth System Research Laboratory Global Monitoring Division and NASA Southern Hemisphere additional ozonesondes; and 3) Real-time Air Quality Modeling System Aura Reanalysis ozone. The independent datasets cover the time period January 2006 through December 2016, and OMPS limb from February 2012 through December 2016.

3.1 ACE-FTS

The Atmospheric Chemistry Experiment (ACE) consists of two instruments onboard the Canadian satellite SciSat, which was launched in August 2003 into a circular orbit at 650 km with a 74° inclination (Bernath et al., 2005b). The instruments on SciSat are the Measurement of Aerosol Extinction in the Stratosphere and Troposphere Retrieved by Occultation (MAESTRO) and the Fourier Transform Spectrometer (FTS) (used by this study). The FTS operates in the 750-4400 cm^{-1} (13.3-2.27 μm) range, and obtains profiles of temperature, pressure, and more than 30 atmospheric trace gases including ozone (Bernath et al., 2005). ACE-FTS obtains profiles at local sunrise (SR) and sunset (SS) through the solar occultation technique. Spectral resolution of the instrument is 0.02 cm^{-1} (Bernath et al., 2005). ACE-FTS has a field of view of 1.25 mrad, a maximum vertical resolution of 3-4 km, and measurements are made from cloud top up to 100-150 km (Bernath et al., 2005). The processing algorithm provides profiles on both a 1 km grid and a varying tangent height retrieval grid (Bernath et al., 2005). This study uses the tangent height measurements. ACE-FTS is generally biased high in comparison

to other measurements, with the version 2.2 ozone retrieval displaying a 1-8% positive bias in the upper troposphere middle stratosphere and a 20% positive bias in the upper stratosphere lower mesosphere (Dupuy et al., 2009). The version 3.6 ozone retrieval is reportedly systematically biased +2% between 10-45 km and 0 to 19% between 46 and 60 km, relative to MLS and the Michelson Interferometer for Passive Atmospheric Sounding (MIPAS) instrument (Sheese et al., 2016).

Throughout the course of a year ACE-FTS samples from 85° N to 85° S, with the majority of retrievals occurring in the polar latitudes (Fig. 1). For the version 3.6 ACE-FTS algorithm there are 48,173 ACE-FTS retrievals available between January 2006 and December 2016. For the current analysis, physically unrealistic outliers are removed using a 5% precision cutoff, a composite Gaussian filter, and a localized filter about a running 15-day median (Sheese et al, 2015). Version 3.6 data is used, as it was the most recent and fully validated version available at the time of our analysis.

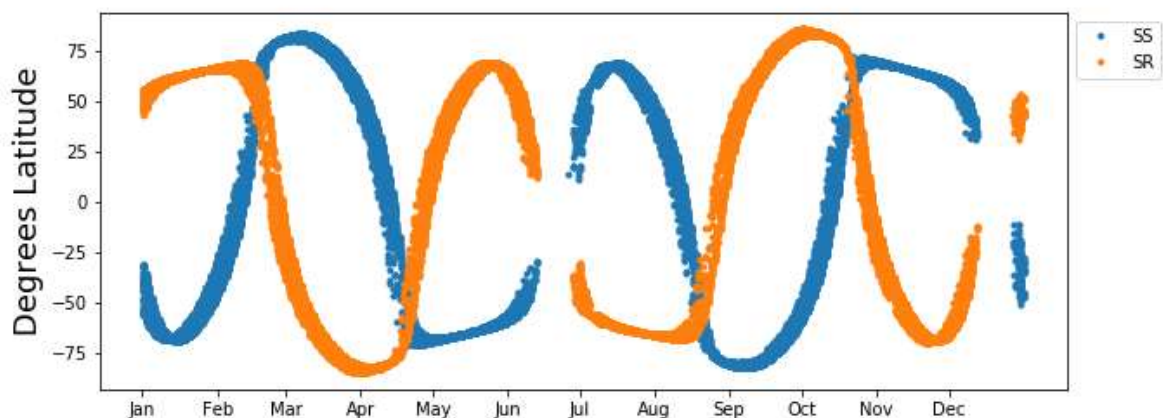


Figure 1. ACE-FTS Annual Sampling by month for SS and SR retrievals. The number of samples is not an annual average, as all latitudes at which an observation was made between January 1, 2006 and December 31, 2016 are plotted.

3.2 Ozonesondes

Ozonesondes are launched from a limited number of sites across the globe and consist of an ozone sensor combined with a traditional meteorological radiosonde. They provide in-situ profiles of ozone concentration, temperature, humidity, and pressure. Ozonesonde measurement error has been estimated as 10% in troposphere, 5% in the stratosphere to 10 hPa, and 5-25% above 10 hPa (Jiang et al 2007). Launch sites and data archival is managed by several organizations, including NOAA Earth System Research Laboratory Global Monitoring Division (ESRL-GMD), NASA Southern Hemisphere additional ozonesondes (SHADOZ), and World Ozone and Ultraviolet Radiation Data Centre (WOUDC).

The most common type of ozonesonde is an electrochemical concentration cell (ECC) with a potassium iodide (KI) solution (Smit et al., 2007). ECCs consist of an anode and cathode cell connected by an ion bridge. Ambient air is bubbled into the cathode cell and the reaction of a molecule of O_3 with the KI solution results in flow of 2 electrons through the ion bridge. Flow across the ion bridge is tracked as the signal for ozone concentration. 35 km is the approximate limit that an ozonesonde typically reaches before the balloon bursts and the ascent phase ends. Ozonesonde quality assurance and standard operating procedures have been carried out under the auspice of the Juelich Ozone Sonde Intercomparison Experiment (JOSIE) project since 1996 (Smit et al., 2007). Locations used in this study are given in Table 1, along with the years of availability and number of profiles available between 2006 and 2016.

NOAA's ESRL-GMD operates several ozonesonde launch sites. These locations include the South Pole, Greenland, Boulder CO, Hilo HI, Huntsville AL, and Trinidad Head CA. NASA/Goddard Space Flight Center operated SHADOZ ozonesondes are located in tropics, subtropics, and southern hemisphere. The most current processing version, version 6, is utilized. While this network spans the globe, this analysis uses three ozonesonde locations in the deep tropics to quantify the differences between RAQMS Aura reanalysis ozone values below the tropical tropopause.

Table 1. Ozonesonde station locations, data providers, and years available during 2006-2016.

Site	Agency	Years used/available	Latitude	Longitude	Number of Profiles
Huntsville, AL	ESRL	2006-2016	34.73 N	86.65 W	632
Summit, Greenland	ESRL	2006-2016	72.58 N	38.46 W	583
Boulder, CO	ESRL	2006-2016	39.95 N	105.20 W	612
Trinidad Head, CA	ESRL	2006-2016	41.06 N	124.15 W	600
Narragansett, RI	ESRL	2006-2011	41.49 N	71.42 W	220
Suva, Fiji	ESRL	2007-2016	18.15 S	178.45 E	141
Natal, Brazil	SHADOZ	2006-2011, 2013-2016	5.49 S	35.26 W	300
Nairobi, Kenya	SHADOZ	2006-2016	1.27 S	36.80 E	447

Kuala Lumpur, Malaysia	SHADO Z	2006-2010, 2012-2016	2.73 N	101.7 E	197
------------------------	------------	-------------------------	--------	---------	-----

3.3 OMPS

The Ozone Mapping Profiler Suite (OMPS) flies onboard the Suomi National Polar-orbiting Partnership (SNPP) satellite. SNPP was launched in October 2011, and scientific data from OMPS reached operational status in 2012 (Kramarova et al., 2018). OMPS consists of two modules: nadir and limb. The nadir module provides both a total column and profile but will be ignored in this study. The limb module consists of a single sensor- the limb profiler. OMPS-L makes two retrievals, one in the visible wavelengths and the other in the UV wavelengths. The UV retrieval provides a profile from 30.5 km to 55.5 km. The visible retrieval is from cloud top (or ~10 km) to 35.5 km.

SNPP makes 14 orbits per day and full global coverage with OMPS-L can be obtained every 3-4 days. Approximately 160 to 180 measurements are taken per orbit, resulting in a sampling distance of about 1° latitude (N. A. Kramarova et al., 2014). Measurements are made from a left, center, and right slit, although only data from the center slit is available. Only center slit data is made available in the NASA version 2.5 data used by this study due to the complexity of accounting for altitude registration offset from the center slit, artificial latitudinal structures, and stray light errors in the left and right slits (Kramarova et al., 2018). Vertical sampling is approximately 1km, with a 1.3-1.7 km field of view (Kramarova et al., 2018).

3.4 RAQMS Aura Reanalysis

The Real-time Air Quality Modeling System (RAQMS) Aura Reanalysis, which extends from 2006 through 2016 is used in this study. RAQMS is a 1x1 degree global model with full stratospheric and tropospheric chemistry driven by the meteorological dynamics of the University of Wisconsin hybrid isentropic coordinate model (Pierce et al., 2007). The RAQMS reanalysis, hereafter referred to as RAQMS-Aura, assimilates ozone monitoring instrument (OMI) total column ozone, microwave limb sounder (MLS) ozone profiles, moderate resolution imaging spectrometer (MODIS) aerosol optical depth (AOD), MODIS fire detections, OMI NO₂, and atmospheric infrared sounder (AIRS) carbon monoxide using the operational grid point statistical interpolation (GSI) 3d var analysis system (R.B. Pierce, personal communication, October 17, 2019). Assimilation of satellite retrievals is performed at six-hour intervals and uses aerosol and chemistry predictions from RAQMS as the background field. RAQMS-Aura provides 1x1° global chemical analyses, on 35 hybrid model levels from the surface to approximately 60 km above ground level, at 3-hour time steps (R.B Pierce, personal communication, October 17, 2019). As the ozone field is constrained by OMI and MLS data, the bias of the model in this field is expected be related to the bias of those instruments (R. B. Pierce, personal communication, October 17, 2019). Aura MLS is known to be biased high, with the retrieval in the lower troposphere not recommended for scientific use (Froidevaux et al., 2008), and uncertainty in the lower portion of the retrieval nearing 20% bias and 5% bias in the UTLS region (Froidevaux et al., 2008; Jiang et al., 2007).

4. Method and Results

4.1 Overview of non-coincident OMPS validation

In this indirect validation scheme, the RAQMS Aura reanalysis is used as an intermediary between observational datasets. RAQMS-Aura ozone is bias-corrected by the median zonal difference of RAQMS-Aura from ACE-FTS observations between 2006 through 2016. This bias correction is a function of latitude and height, and its application limited to above the tropopause. ESRL and SHADOZ ozonesondes during the same time period are used in two ways: 1) to validate the bias correction to RAQMS-Aura above the tropopause; 2) to assess the accuracy of RAQMS-Aura below the tropopause. Following application of the bias correction, RAQMS-Aura is used to describe zonal mean and seasonal biases in the OMPS limb profiler UV and visible ozone profile retrievals. This method allows for use of all valid measurements, not just those that happen to be coincident with another measurement, resulting in a more statistically robust calculation of the bias in OMPS limb profiler retrievals than direct methods.

4.2 ACE-FTS Analysis and Bias Correction of RAQMS-Aura

The solar occultation limb sounder ACE-FTS instrument makes profile measurements of ozone with low sampling frequency and high vertical resolution. Due to its high precision and vertical resolution, this study chose to use ACE-FTS ozone profiles as the baseline for evaluating accuracy of the stratospheric ozone concentration in the RAQMS-Aura reanalysis. This analysis is done over the entire 2006-2016 data range and does not include any accounting for seasonal timescale variation, as the ACE sampling pattern makes a meaningful global seasonally varying quantification of the bias between RAQMS-Aura and ACE-FTS difficult. Filtering was necessary to remove extreme values, as they greatly influenced the mean and spread statistics.

Median average deviation (MAD) and median were calculated separately for the sunset (SS) and sunrise (SR) retrievals (and associated RAQMS-Aura). While validation of a previous processing version of ACE-FTS ozone retrievals (version 2.1) found no systematic bias between SR and SS measurements (Dupuy et al., 2009), they are initially evaluated separately here to check behavior of RAQMS-Aura is not systematically different at SR vs SS. A bias correction for RAQMS-Aura ozone concentrations is defined as the zonal median difference from all valid ACE-FTS retrievals within pressure and latitude bins.

4.2.1 Removal of Physically Unrealistic Outliers from ACE-FTS

RAQMS-Aura is sampled within 1.5 hours, 0.5° longitude, and 0.5° latitude of each ACE-FTS retrieval. Coincident RAQMS-Aura profiles are linearly interpolated to ACE-FTS measurement pressure levels. Preliminary data screening rejects measurements for which the ACE-FTS signal to noise ratio exceeds 5%. This preliminary screening does not remove all unphysical observations and so additional screening must be applied. Physically unrealistic outliers are removed from the ACE-FTS SS and SR datasets using the two step procedure outlined in Sheese et al., 2015.

The two-step outlier removal procedure is applied as follows: Extreme outliers are removed first by rejecting points outside the 95% confidence intervals on a composite Gaussian fit for each pressure level and latitude region. The composite Gaussian fitting procedure may use a maximum of three Gaussians and ignores the five highest and lowest values in each pressure-latitude region. There are 4 latitude regions for which this is done: a) $60\text{-}90^\circ$ S; b) $0\text{-}60^\circ$ S; c) $0\text{-}60^\circ$ N; d) $60\text{-}90^\circ$ N. These regions were selected

following those chosen by Sheese et al., 2015 where an approximately equal number of ACE-FTS profile observations between 2004 and 2013 fell within each region and the distribution was at most tri-modal. Next, local outliers are removed for each pressure-latitude region through application of a filter about a 15-day running median. In this step, observations within the aforementioned regions and outside ± 10 times the mean absolute deviation about the median (MeAD) of the median are discarded. MeAD is a variant of the median absolute deviation (MAD) intended to be more sensitive to outliers and is defined as:

$$\frac{1}{n} \sum_{i=1}^n |x_i - x_j|$$

where n is the number of observations in the 15-day period and x_j is the 15-day median.

Following removal of physically unrealistic outliers, the remaining ACE-FTS data and coincident RAQMS-Aura is grouped by 2° latitude and AIRS 100 pressure levels. The AIRS 100 pressure levels have a log10 spacing between 1000 hPa and 0 hPa with 10 levels per decade of pressure.

4.2.2 Bias in RAQMS-Aura relative to ACE-FTS Sunrise Retrievals

Zonal median ozone concentration for ACE-FTS SR and the coincident RAQMS-Aura is displayed in Fig. 2. Overall, the two datasets display a similar distribution as would be expected. However, there are some significant differences at low pressure (high altitude) and about 10 hPa in the tropics where ozone concentration is at a peak globally. The median ozone concentration for the ACE-FTS SR retrievals near 10 hPa between 20° S and 20° N is approximately 10-11 ppmv. The shape of this ozone maximum is similar

in the coincident RAQMS-Aura median but is about 1 ppmv lower in magnitude. This indicates an underestimate of ozone concentration by the model in this region. The median concentrations near the top of the retrievals displays a tendency of RAQMS-Aura to overestimate ozone at these altitudes. These features are confirmed in Fig. 3a, which displays the median difference in concentration between ACE-FTS SR and RAQMS-Aura. The median difference in concentration reveals that RAQMS-Aura is generally biased low in comparison to ACE-FTS SR.

The zonal MAD for ACE-FTS SR and coincident RAQMS-Aura is given in Fig. 4. It is below about 0.5 ppmv for most of the domain in both datasets. Below 1 hPa the MAD is similar for ACE-FTS and RAQMS-Aura, although there are small regions for which the two differ by about 0.1 ppmv. Above 1 hPa the difference in MAD between RAQMS-Aura and ACE-FTS SR is more widespread. Poleward of 60° RAQMS-Aura displays increased variance in concentration compared to ACE-FTS, while equatorward of 60° RAQMS-Aura displays decreased variance compared to ACE-FTS.

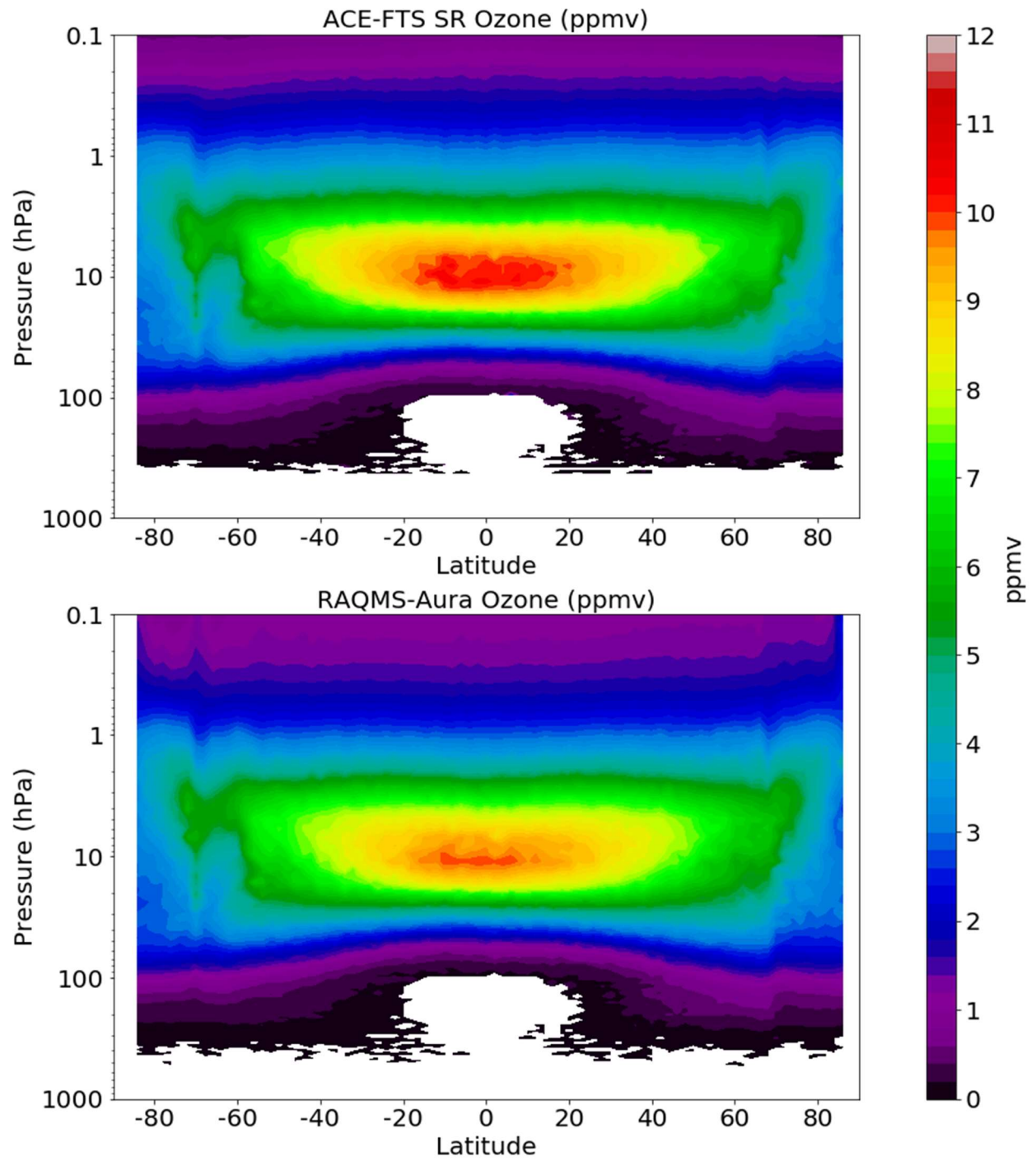


Figure 2. ACE-FTS SR and RAQMS-Aura Zonal Median ozone concentration in ppmv.

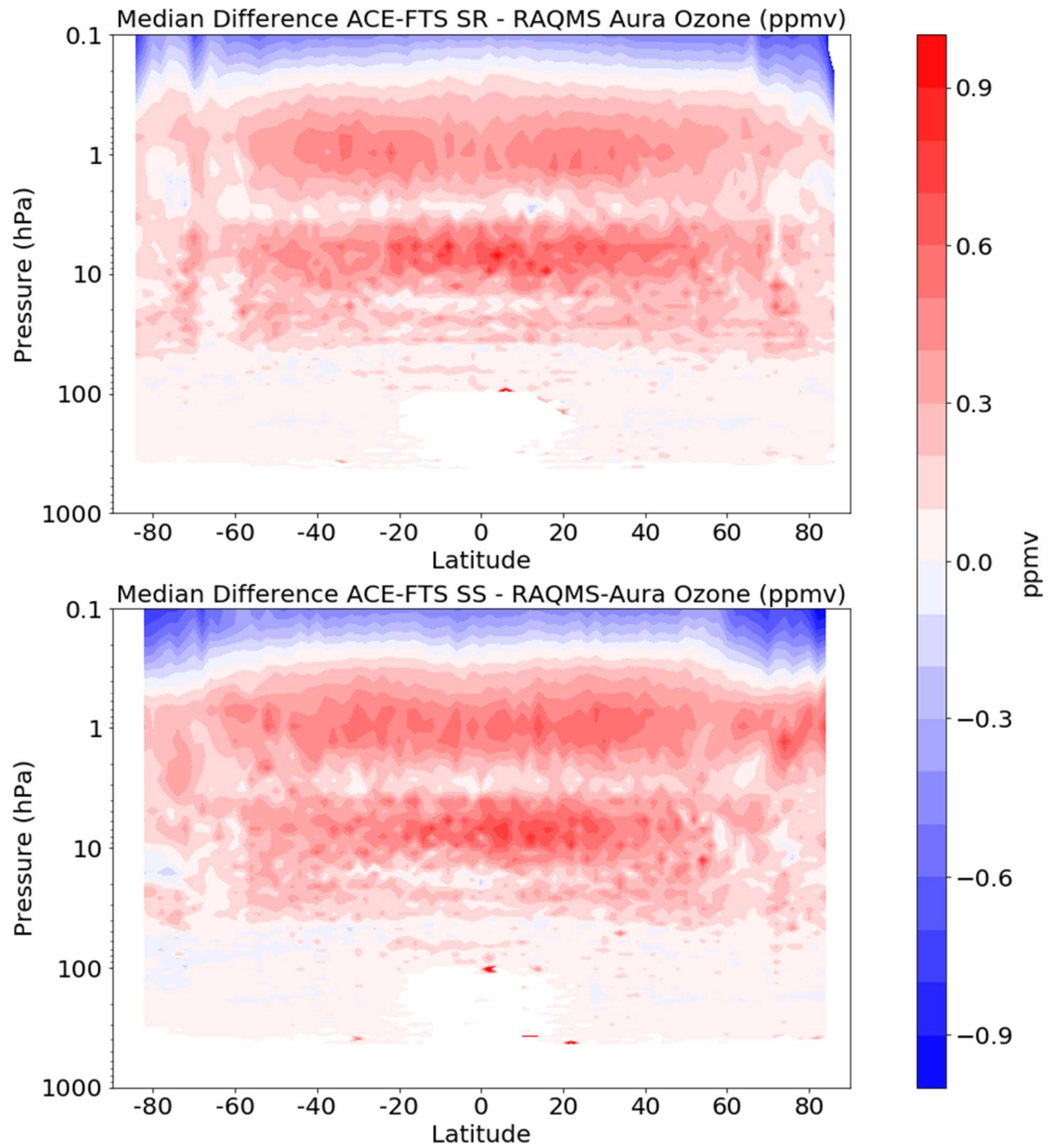


Figure 3. Difference in ppmv between ACE-FTS retrieval median and RAQMS Aura median for the entire 2006-2016 time period.

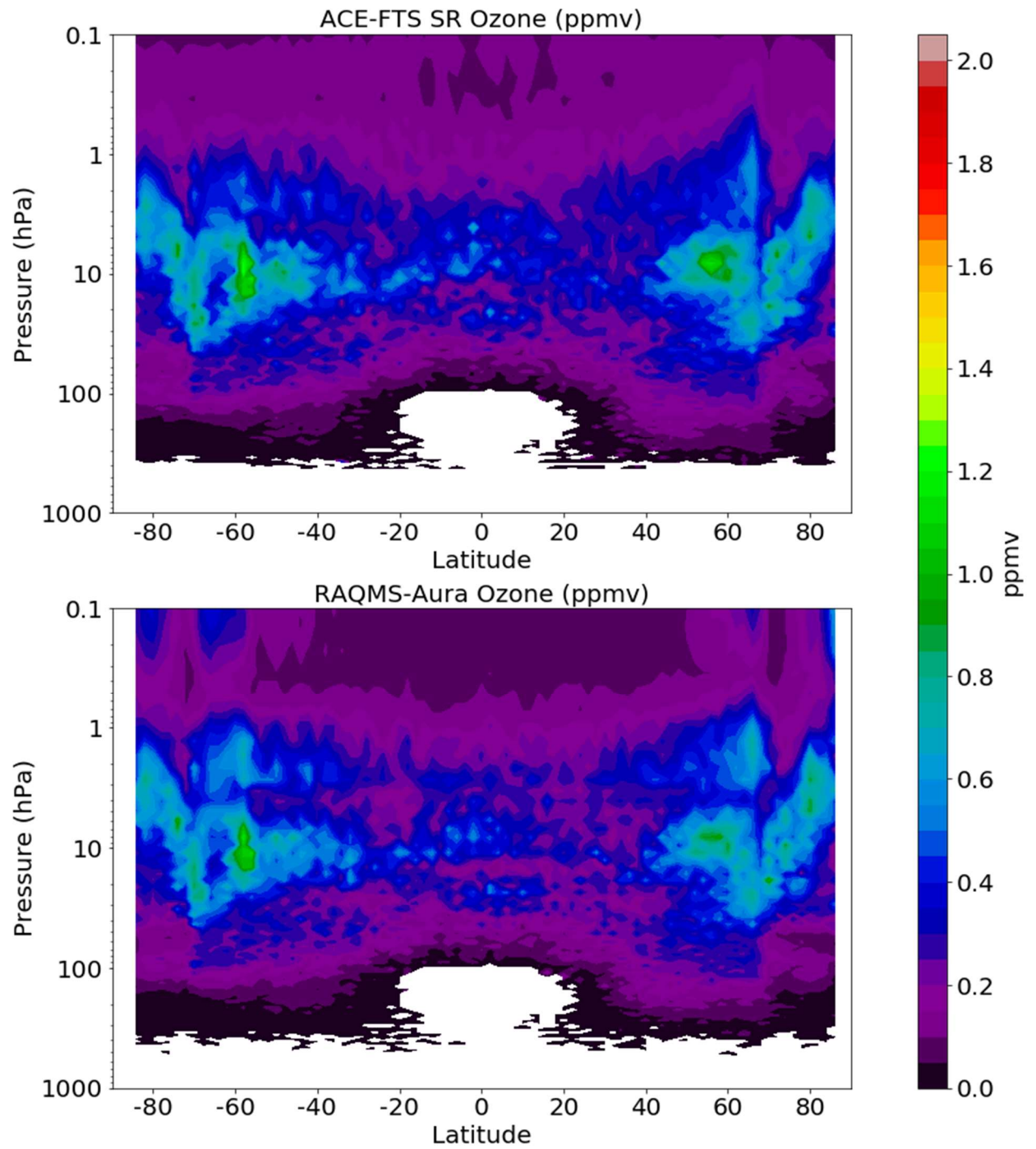


Figure 4. Median absolute deviation in ppmv for ACE-FTS SR and coincident RAQMS-Aura.

4.2.3 Bias in RAQMS-Aura relative to ACE-FTS Sunset Retrievals

Zonal median ozone concentration for ACE-FTS SS and the coincident RAQMS-Aura is displayed in Fig. 5. The general shape is similar to that previously seen with the SR retrievals, except for the regions poleward of 60° N and 60° S. As with the SR retrievals, the observed and modeled median concentrations differ about 10 hPa in the tropics and at low pressure (high altitude). Underestimation of the peak ozone concentration near the tropics is lessened in this case compared to the SR case, albeit slightly. The median difference in concentration between ACE-FTS SS and RAQMS-Aura is given in Fig. 3b. The median difference again reveals a general low bias in RAQMS-Aura. In comparison to the difference calculated for RAQMS-Aura and the SR retrievals, RAQMS-Aura varies from the SS retrieval a little differently poleward of 60° N (S). RAQMS-Aura is biased high near uniformly above 0.2 hPa. Below 0.2 hPa, RAQMS-Aura is generally biased low in comparison to ACE-FTS SS. Poleward of 60° N, RAQMS-Aura is biased low with a stronger bias between 1 and 0.16 hPa than in the SR case. Poleward of 60° S, RAQMS-Aura displays a stronger bias than in the SR case.

The zonal MAD for ACE-FTS SS and coincident RAQMS-Aura is given in Fig. 6. It is below about 0.5 ppmv for most of the domain in both datasets. Below 1 hPa the MAD is similar for ACE-FTS and RAQMS-Aura, although there are small regions for which the two differ by about 0.1 ppmv. Above 1 hPa the difference in MAD between RAQMS-Aura and ACE-FTS SS is more widespread. Poleward of 60° RAQMS-Aura displays increased variance in concentration compared to ACE-FTS, while equatorward of 60° RAQMS-Aura displays decreased variance compared to ACE-FTS.

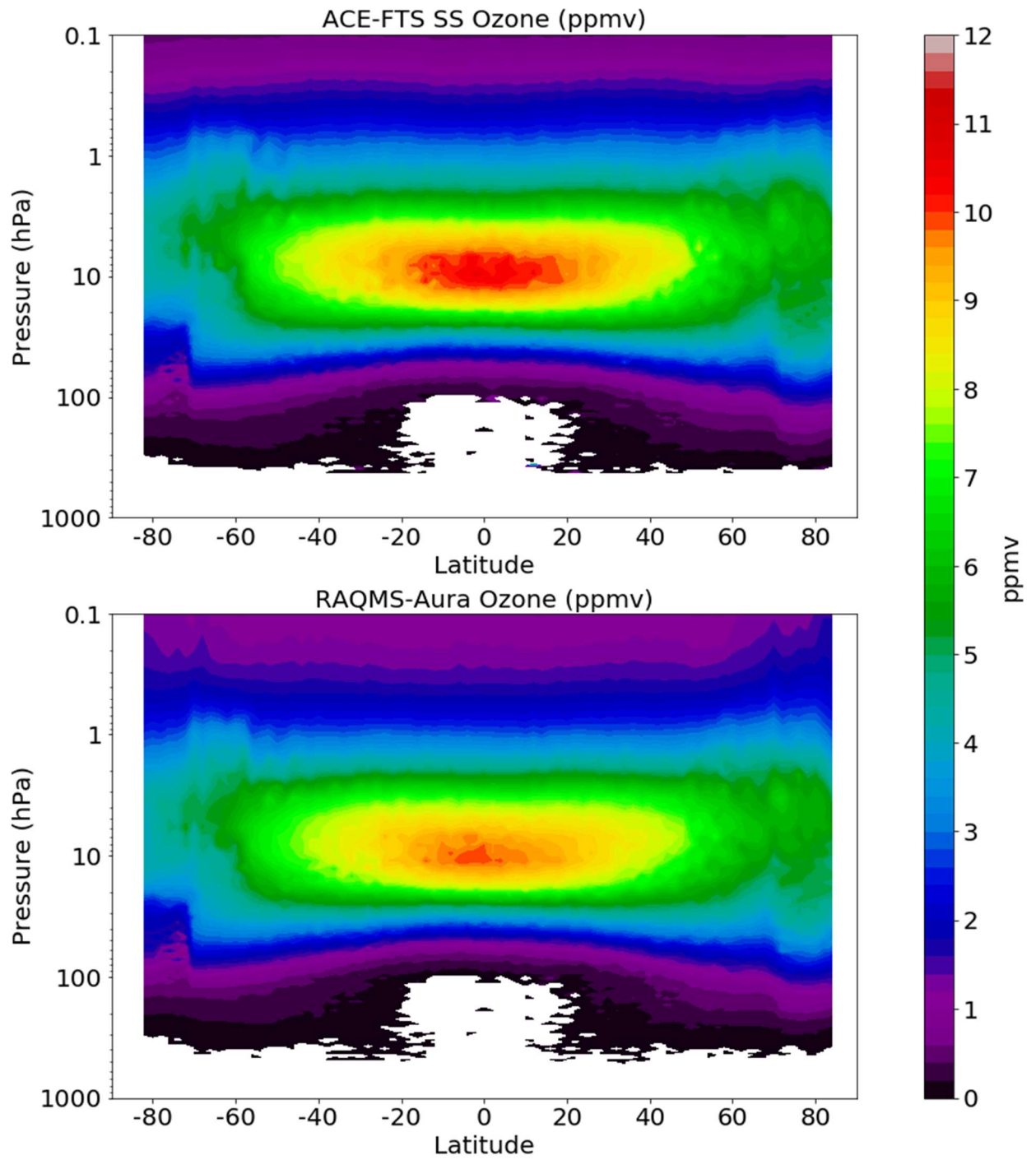


Figure 5. ACE-FTS SS and RAQMS-Aura Zonal Median ozone concentrations in ppmv.

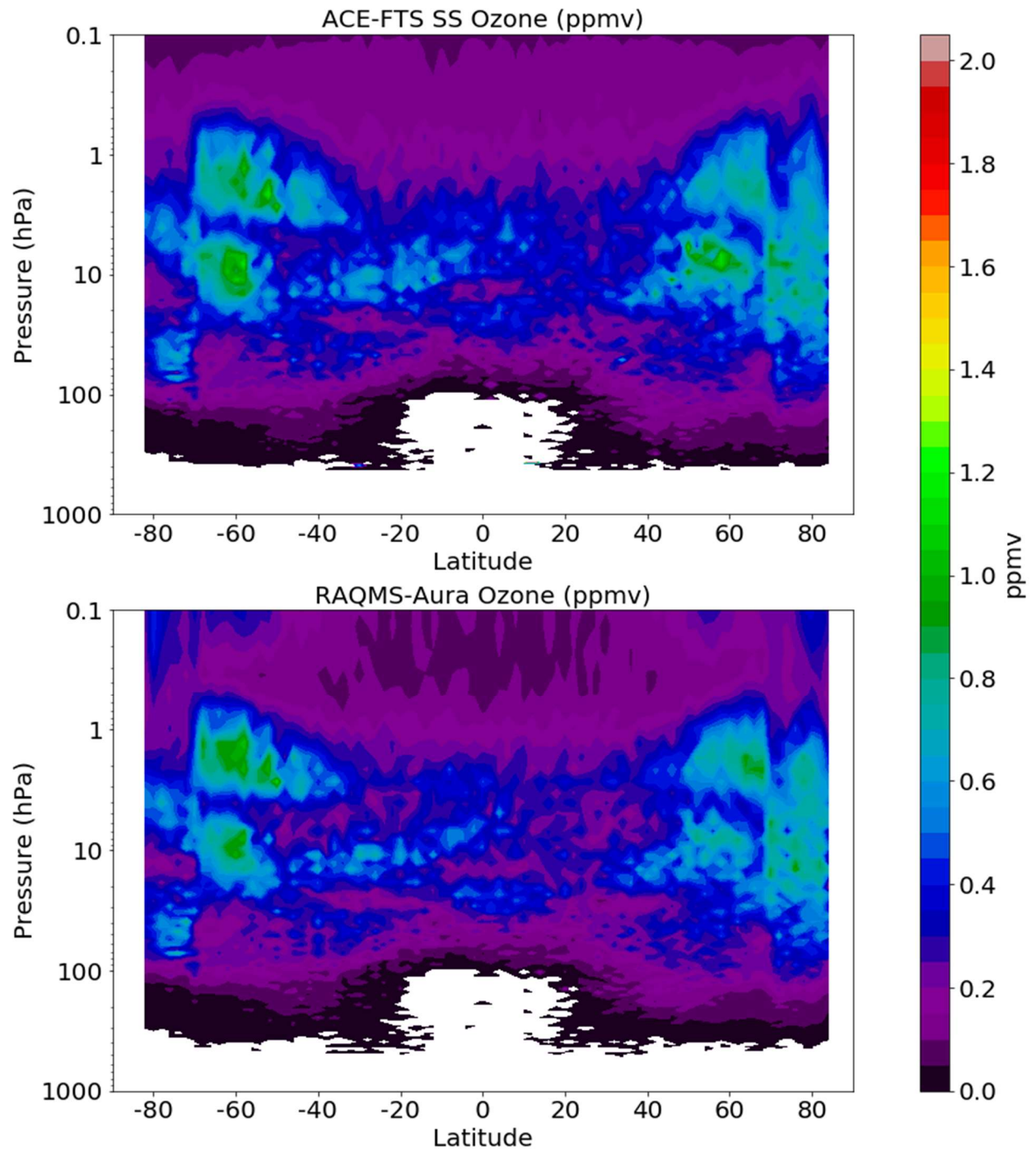


Figure 6. Median absolute deviation in ppmv for ACE-FTS SS and coincident RAQMS-Aura.

4.2.4 RAQMS-Aura Bias Correction

The differences between the zonal median difference for the SR and SS cases are strongest in the polar regions. While this could be indicative of RAQMS-Aura mis-capturing a diurnal cycle in ozone, hemispheric seasonal variation in ozone should not be discounted as ACE-FTS SS and SR sampling of the polar regions does not occur simultaneously. The SS measurement is made near the poles during the first two months of spring in both hemispheres. The SR measurement does capture the polar regions just before meteorological spring but does not observe as far poleward as SS does during the peak ozone loss period. RAQMS-Aura captures global mean variation in total column ozone well but does struggle with fine scale variation and the magnitude and altitude of the ozone hole. Resulting from the modeling deficiency and ACE-FTS sampling pattern, it is plausible that the observed differences in zonal median difference are due to seasonal processes such as the ozone hole.

While there are obvious differences in agreement between RAQMS-Aura ozone concentrations and ACE-FTS SS and SR ozone retrievals in the polar regions, the median zonal differences between 60° S and 60° N are of a similar magnitude and shape (Fig. 13). The RAQMS-Aura reanalysis does capture the variance observed by ACE-FTS reasonably well, as evident in comparisons of MAD, and so the reanalysis is suitable for use in the indirect validation of OMPS-L following a bias correction. Combining the difference from ACE-FTS observations in RAQMS-Aura for the SS and SR retrievals into a single zonal mean difference results in a better depiction of the 11-year zonal median bias of RAQMS-Aura ozone concentrations than using SS or SR alone. This combined difference is displayed in Fig. 7. This bias correction is applied only above the

model tropopause and when the composite encompasses more than twenty observations. Twenty was chosen as the criterion for the number observations per latitude/pressure bin during the 11-year observational period that a representative median value could be generated based on the sampling pattern of ACE-FTS (Fig. 1). This is enforced through setting the zonal median difference to zero where the criterion is not met.

Application of the bias correction is done profile by profile for RAQMS-Aura coincident with ozonesondes or OMPS limb measurements. The bias correction is applied by first linearly interpolating the ACE-FTS/RAQMS-Aura zonal median difference to the latitude and pressure of the selected RAQMS-Aura profile. This difference is then added to the RAQMS-Aura profile above the tropopause to result in a bias-corrected profile.

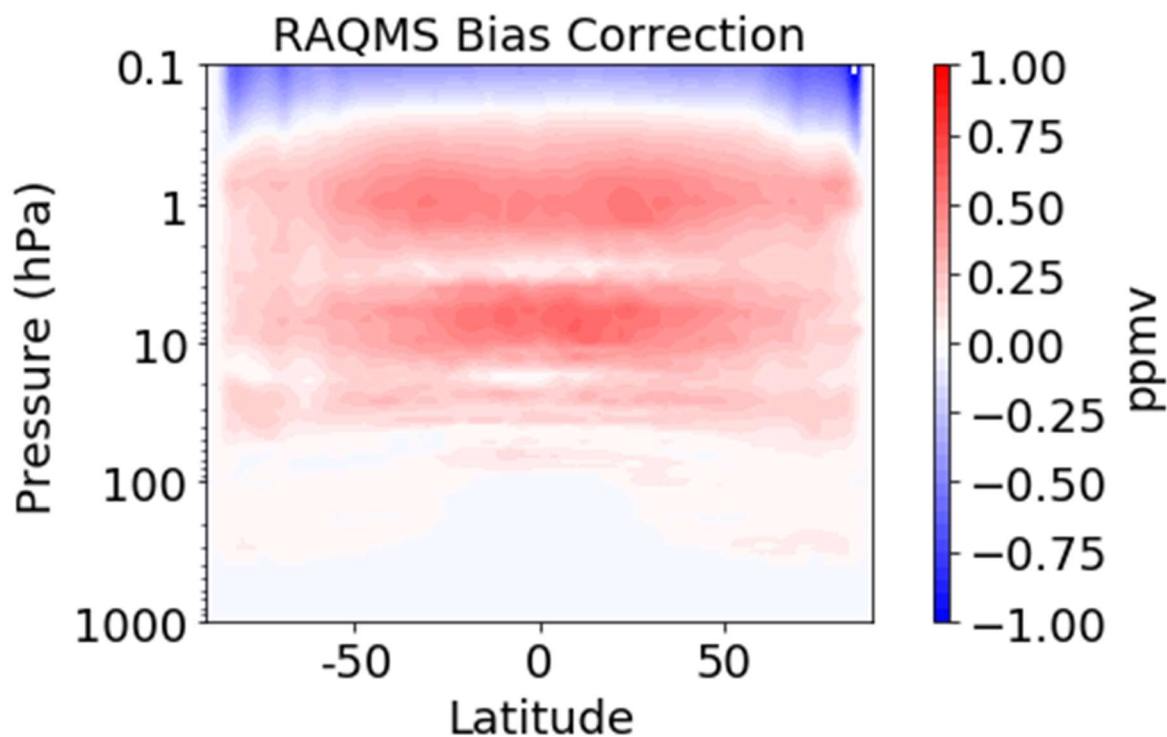


Figure 7. Bias Correction for RAQMS-Aura. Derived from median ACE-FTS SS and SR difference with coincident RAQMS-Aura.

4.3 Ozonesondes

Ozonesondes collect measurements from ground level to around 30 km. This altitude range is partly covered by satellite profile retrievals, as profilers can obtain retrievals down to near 10 km in the absence of cloud cover and to cloud top otherwise. Ozonesonde profiles have a high vertical resolution, with most reported profiles giving a measurement around every 100 m. Validation using only ozonesondes is limited due to the small number of ozonesonde launch locations and low launch frequency. The NOAA ESRL and NASA SHADOZ ozonesonde networks together consist of 27 ozonesonde sites. The 9 sites used in this study are listed in Table 1. Three SHADOZ sites spanning the deep tropics with availability covering 2006-2016 were selected for evaluating the model bias in the tropics. The launch frequency for most ozonesonde locations is a week or more.

Bias and correlation by location, ESRL ozonesondes, and SHADOZ ozonesondes is evaluated for three groupings: 1) all measurements; 2) ozonesonde measurements less than 200 ppbv; and 3) ozonesonde measures greater than 1 ppmv. The divisions of 200 ppbv and 1 ppmv separate tropospheric and stratospheric ozone. Correlation and bias between RAQMS-Aura and an ozonesonde site are calculated before and after application of the bias correction. The correlation and bias are presented in Table 2. Scatter plots are used to look at the correlation between the ozonesonde and RAQMS. Impact of the ACE bias correction is also investigated with a scatter plot of the

magnitude of the correction compared to ozonesonde observation. Average percent bias is evaluated by altitude and distance from the tropopause.

Table 2. Pearson Correlation between ozonesondes and coincident RAQMS Aura simulated Ozone mixing ratio.

	Corrected R	Corrected bias	Uncorrected R	Uncorrected bias
All	0.996	233.159	0.996	236.819
All < 200 ppbv	0.779	28.887	0.774	26.963
All > 1 ppmv	0.988	367.261	0.987	374.492
ESRL	0.995	226.502	0.995	240.444
ESRL < 200 ppbv	0.746	32.630	0.737	30.681
ESRL > 1 ppmv	0.986	368.155	0.985	344.843
Tropics	0.997	250.728	0.997	226.444
Tropics < 200 ppbv	0.858	19.202	0.870	17.132
Tropics > 1 ppmv	0.991	437.194	0.991	396.017
Alabama	0.997	209.965	0.997	225.729
Alabama <200ppbv	0.641	40.578	0.623	38.795
Alabama >1ppmv	0.989	333.154	0.989	361.519
Greenland	0.993	220.805	0.993	252.717
<200 ppbv	0.808	31.055	0.806	22.909
>1 ppmv	0.978	299.826	0.977	346.164
Boulder	0.995	237.342	0.995	239.626
<200 ppbv	0.840	23.595	0.833	22.555
> 1 ppmv	0.985	365.152	0.985	369.444
Trinidad Head, CA	0.995	234.061	0.995	250.527
< 200 ppbv	0.835	26.081	0.830	25.161
> 1 ppmv	0.985	362.992	0.984	390.902
Rhode Island	0.995	239.4907	0.995	234.529
< 200 ppbv	0.538	48.1699	0.530	47.040
> 1 ppmv	0.985	367.2763	0.985	359.571

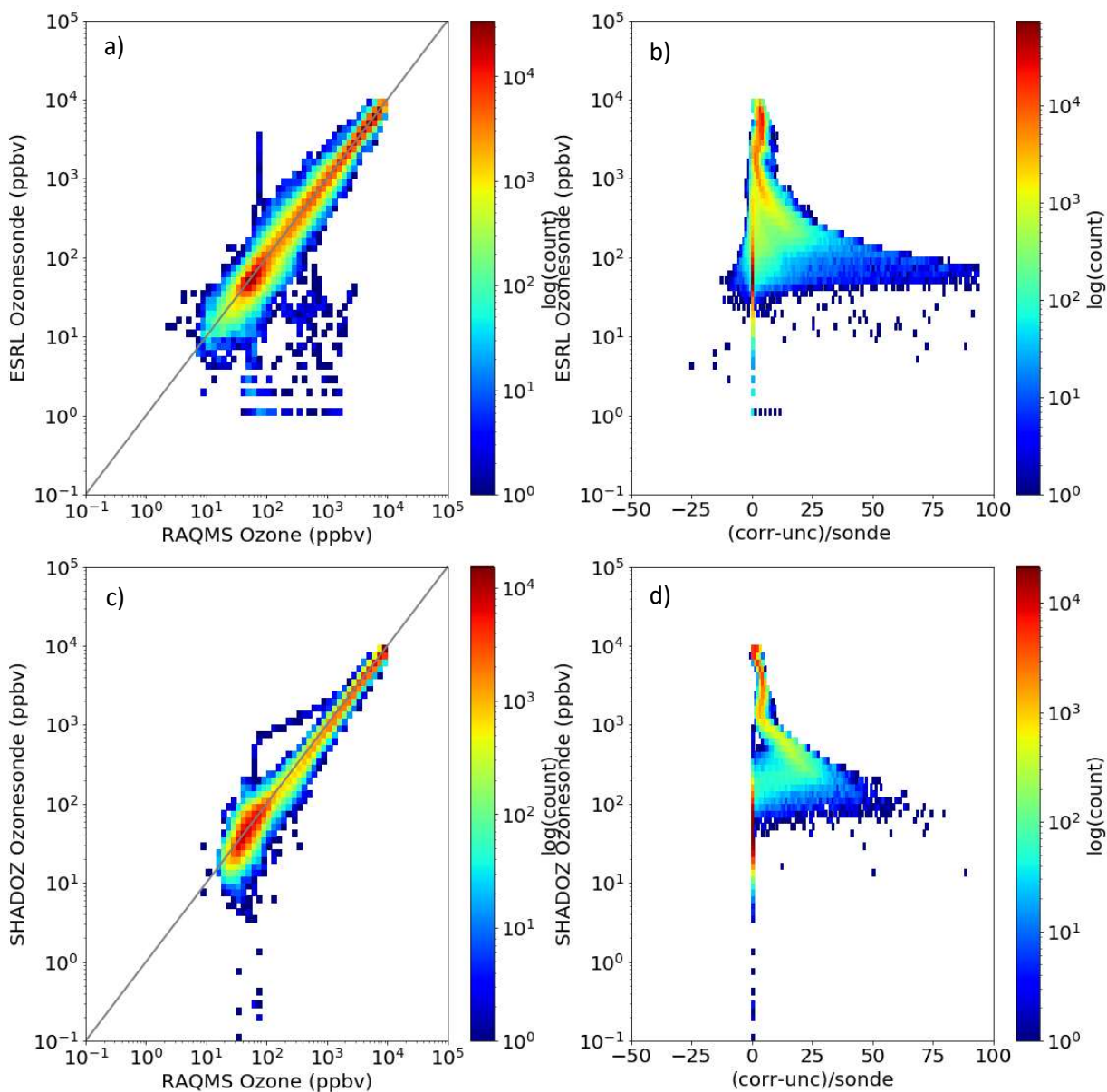


Figure 8. Scatter plots showing (left) the relationship between ozonesonde measurements and corrected RAQMS Aura values and (right) magnitude of the correction as percentage of the ozonesonde value.

4.3.1 ESRL ozonesondes

Fig. 8a displays the relationship between ESRL ozonesonde measurements and the bias corrected coincident RAQMS-Aura values. The calculated bias relative to the entire profile is 226.502 ppbv and the correlation is 0.995. The linear relationship

between ESRL measurements and corrected RAQMS-Aura concentrations is represented by the regression line $y = 1.000x + 21.115$, indicative of a nearly 1:1 relationship.

Correlation of the uncorrected RAQMS-Aura concentrations and ESRL measurements is the same to 3 decimal places as for the corrected RAQMS-Aura case, and so we are not losing a mean agreement between ozonesonde measurements and RAQMS-Aura as a result of the correction. Bias decreases with application of the correction, from 240.444 ppbv to 226.502 ppbv. The impact of the correction is displayed in Fig. 8b as the magnitude of the correction as a percentage of the ozonesonde measurement. The major impact of applying the correction is an increase, which is consistent with the bias correction presented in Fig. 7. Over 99% of the corrections are less than 25% of the observed concentration. The impact of the correction is much more varied for measurements between 100 ppbv and 1 ppmv, with a few measurements corrected by an excess of 50% of the ozonesonde measurement.

To calculate an approximate tropospheric bias in the model, bias and correlation were calculated for when the ozonesonde measured less than 200 ppbv. These values are given in Table 2 for the corrected RAQMS-Aura as a bias of 32.630 ppbv and correlation of 0.746. This bias represents 16% or greater of the ozonesonde measurement, and is a high bias as seen in Fig. 8a.

Now we will look at the bias in RAQMS-Aura concentrations relative to ESRL ozonesonde measurements as a function of altitude, displayed in Fig. 9. The model tropopause for the coincident RAQMS-Aura profiles ranges between 5.8 km and 19.2 km. Above 2 km, the corrected RAQMS-Aura concentrations are on average within 7.5%

of the ESRL measurement. Larger high biases are found below 2 km. At many altitudes application of the correction factor on average decreases the magnitude of the bias in RAQMS-Aura. Above 10 km the average bias by altitude of the corrected RAQMS-Aura is less than 5% and is positive. Prior to applying the correction factor, RAQMS-Aura displayed an average negative bias relative to ACE-FTS ozone concentrations and ESRL ozonesonde measurements. Following application of the correction, RAQMS-Aura displays an average positive bias relative to the ESRL ozonesonde measurements. The magnitude of bias does increase slightly for the altitude regions 7.5-10 km and 16-20 km, but decreases for all other altitude regions. While there is a remaining slight high bias relative to ozonesondes following application of the correction factor, the correction factor does reduce the average magnitude of the bias where tested.

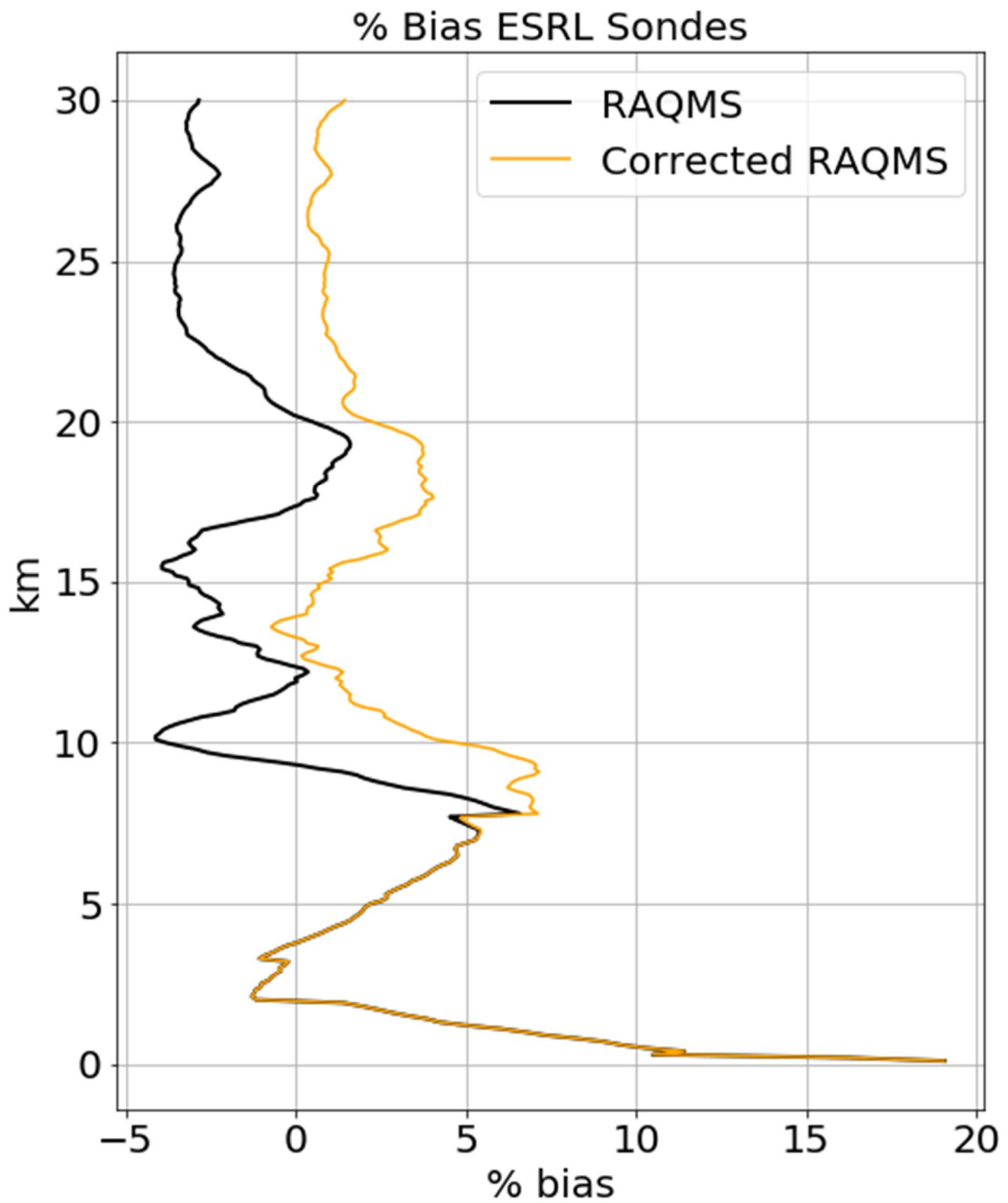


Figure 9. Average percent bias between all ESRL ozonesonde profiles and coincident RAQMS-Aura profiles.

4.3.2 SHADOZ Ozonesondes

The combined three deep tropics stations are used to look at the general behavior of reanalysis in the tropics, particularly below the tropical tropopause. The SHADOZ measurements and RAQMS-Aura are on average in agreement, although RAQMS-Aura underestimates ozone concentration for ozonesonde measurements less than 100 ppbv (Fig. 8c). To calculate an approximate tropospheric bias in the model, bias and correlation were calculated for when the ozonesonde measured less than 200 ppbv. These values are given in Table 2 for the corrected RAQMS-Aura as a bias of 19.202 ppbv and correlation of 0.858. The linear relationship between SHADOZ measurements and corrected RAQMS-Aura concentrations is represented by the regression line $y = 1.025x + 27.847$, indicative of a near 1:1 relationship with a slight overestimation by RAQMS-Aura. The correlation between RAQMS-Aura concentrations and SHADOZ ozonesondes is unchanged following the correction at 0.997 in both cases. The bias increases following the correction from 226.444 ppbv to 250.728 ppbv.

We can better pinpoint where this increased bias following application of the correction factor is likely occurring by looking at the bias as a function of altitude. In the tropics for the majority of the ozonesondes a concentration of at least 1 ppmv is first observed near 20 km. Percent bias in coincident RAQMS-Aura profiles as a function of altitude above ground level is given in Fig. 10. Below about 17 km no change in percent bias occurs following application of the correction factor, consistent with no adjustment below the model tropopause. Above 17 km, an overall increase in bias is seen, with the largest increase occurring between 17 km and 20 km. Excluding the lowest 3 km and the

17-20 km range, the corrected RAQMS-Aura is biased 0-10% high with respect to the SHADOZ ozonesondes with bias at most altitudes within 5%. Percent bias in coincident RAQMS-Aura profiles as a function of distance from the tropopause is given in Fig. 11. The RAQMS-Aura tropopause is defined following the World Meteorological Organization (WMO) thermal tropopause definition, where the tropopause occurs at the lowest level at which the lapse rate is $2^{\circ}\text{C}/\text{km}$ or less and the 2km average lapse rate is less than $2^{\circ}\text{C}/\text{km}$. The model tropopause at the selected SHADOZ locations during the observed days is between 15 km and 19 km, with the mean model tropopause at 16.9 km. Between 0.5 km and 5 km below the tropopause, the corrected RAQMS-Aura is biased $\sim 0-7.5\%$ higher than SHADOZ measurements. Between 0.1 km below the tropopause and 3 km above the tropopause, corrected RAQMS-Aura concentrations are biased 10% to 17.5% higher than SHADOZ measurements.

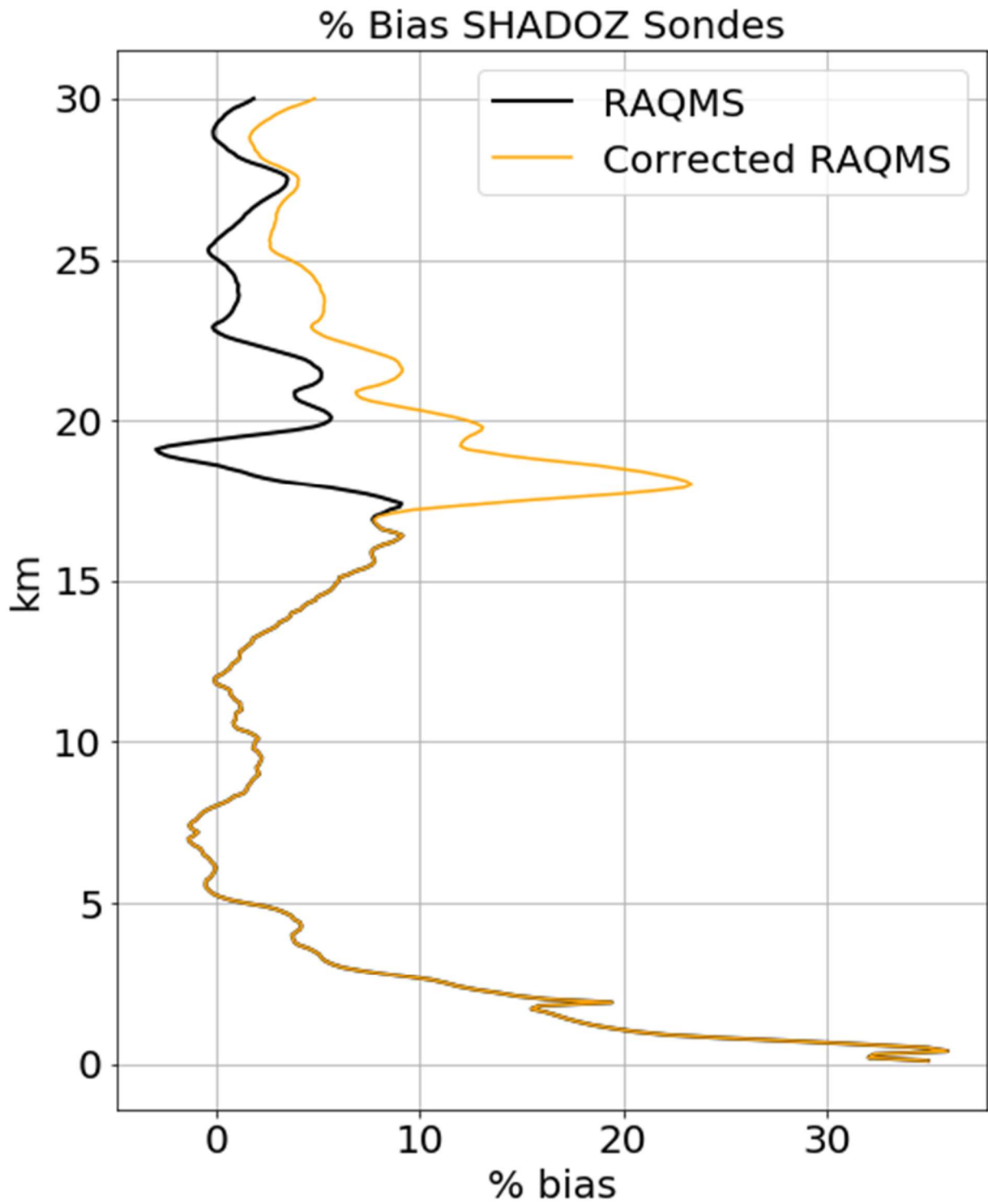


Figure 10. Bias, expressed in percent, between RAQMS-Aura and SHADOZ ozonesonde measurements. SHADOZ sites at Natal Brazil, Nairobi Kenya, and Kuala Lumpur Malaysia were used.

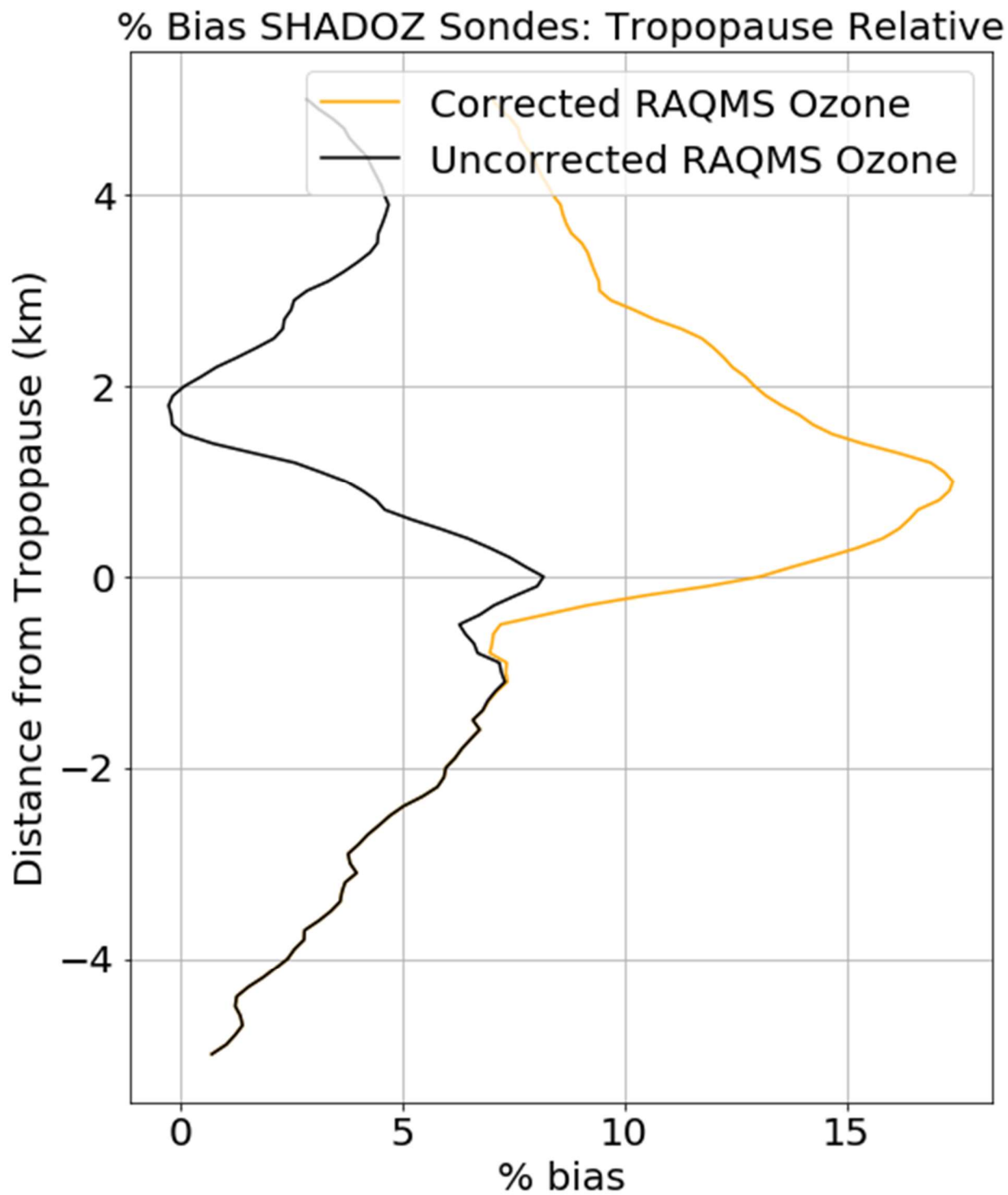


Figure 11. Profile of percent bias of RAQMS-Aura to SHADOZ ozonesonde measurements, expressed as a function of altitude from tropopause. SHADOZ sites at Natal Brazil, Nairobi Kenya, and Kuala Lumpur Malaysia.

4.3.3 Summary of Ozonesonde analysis

Comparisons between the ACE bias corrected RAQMS-Aura ozone and ozonesondes shows that the application of bias correction increases RAQMS-Aura ozone concentration on average as intended. Application of the correction factor to RAQMS-Aura on average decreases the bias relative to the ozonesondes above the model tropopause for the ESRL ozonesonde sites. For the deep tropics SHADOZ sites an increase in bias above the tropopause relative to the ozonesondes is seen following application of the correction factor. For all sites the corrected RAQMS-Aura is on average within +0-10% of the ozonesonde measurements, excluding below 2 km and 17-20 km in the deep tropics. Since the ACE-FTS derived correction factor is applied only above the model tropopause, the tendency of RAQMS-Aura below the tropopause is limited to what can be gleaned from the ozonesonde comparison. These comparisons with ozonesondes shows that the bias corrected RAQMS-Aura ozone has a high bias of up to 10% in the tropical lower stratosphere and a high bias of 0-5% elsewhere. For the analysis performed in this study, the bias of RAQMS-Aura is relatively unimportant lower than ~10 km, as OMPS-L retrievals are performed below cloud top and are limited to about 10 km in the absence of clouds.

4.4 OMPS-L Validation

Initial calibration and validation activities for the instrument Sensor Data Record (SDR) and Environmental Data Record (EDR) algorithms used internal consistency metrics to determine that the performance of OMPS-L meets the original design criteria (Jaross et al., 2014). A case study of the 2012 Antarctic Ozone hole used MLS profiles, OMPS Nadir profiler retrievals, and an ozonesonde to validate the OMPS-L retrievals

used in the study (N. A. Kramarova et al., 2014). A direct validation of OMPS-L over a longer time frame (April 2012-2017) and the entire globe has been carried out (Kramarova et al., 2018). These direct validations characterize OMPS bias to be within approximately $\pm 10\%$ of other measurements (Kramarova et al., 2014). This study uses indirect validation to increase the robustness of the bias calculations and compares the calculated bias statistics to those obtained by Kramarova et al 2018.

For each OMPS-L profile retrieval, a coincident RAQMS-Aura profile is obtained through selecting the RAQMS-Aura analysis valid within ± 1.5 hours of the retrieval and interpolating the analysis to the retrieval latitude, longitude, and altitudes. The previously calculated bias correction is applied above the tropopause to the RAQMS-Aura profile. For both the visible and UV retrieval, zonal mean percent difference between OMPS-L and RAQMS-Aura profiles are evaluated for: 1) 5° latitude bins; and 2) wide latitude bins. The wide latitude bins used (for consistency with Kramarova et al 2018) are a) 90° - 60° S; b) 60° - 20° S; c) 20° S- 20° N; d) 20° - 60° N; e) 60° - 90° N.

4.4.1 Visible Retrieval

The 5° latitude bin-1 km altitude zonal mean percent difference is given in Fig. 12a. The zonal mean percent difference between the OMPS-L visible retrieval and corrected RAQMS-Aura is primary slightly negative. The percent difference is within $\pm 10\%$ throughout nearly the entire domain, excluding the tropics below 20 km. The region below 20 km in the tropics is characterized in the retrieval by an anomalous high bias in excess of $+40\%$. The tropical troposphere bias in the Kramarova et al. 2018 OMPS-L validation is greatly negative in this area for both the OSIRIS and MLS comparisons. Based on our ozonesonde analysis in section 3.3 of this thesis, RAQMS-

Aura is known to be biased high about the tropical tropopause by 2-17%. Because of this, the actual bias in OMPS-L visible retrieval for the tropical troposphere is likely to be larger than calculated and the low bias in OMPS-L just above the tropical tropopause is likely to be closer to zero than calculated (Fig. 12a). This also suggests that the MLS and OSIRIS retrievals in the tropical troposphere must be biased even higher relative to ozonesondes than OMPS-L and RAQMS-Aura. Outside of the tropical troposphere, the calculated bias in OMPS-L is similar to the Kramarova et al 2018 MLS relative bias (not shown). The calculated bias here are slightly more negative than the prior validation.

Profiles of the percent difference between the OMPS-L visible retrievals and corrected RAQMS-Aura over the wide latitude bands is given in Fig. 13. The percent difference is largest below 20 km between 20° S and 20° N. Between 20° S and 20° N above 20 km the percent difference is between -10% and 0%. Between 60° and 90° S, the percent difference is smallest near retrieval base and largest near retrieval top. OMPS-L concentration is on average less than the RAQMS-Aura concentration, with the percent difference approximately between -15 and 0%. Between 60° and 20° S OMPS-L is biased lower than RAQMS-Aura. The percent difference is near -15% near retrieval base and decreases to -2% near retrieval top. Between 20° and 60° N OMPS-L is biased between -10 and 0% lower than RAQMS-Aura. Between 60° and 90° N OMPS-L is biased between -15 and -5% lower than RAQMS-Aura.

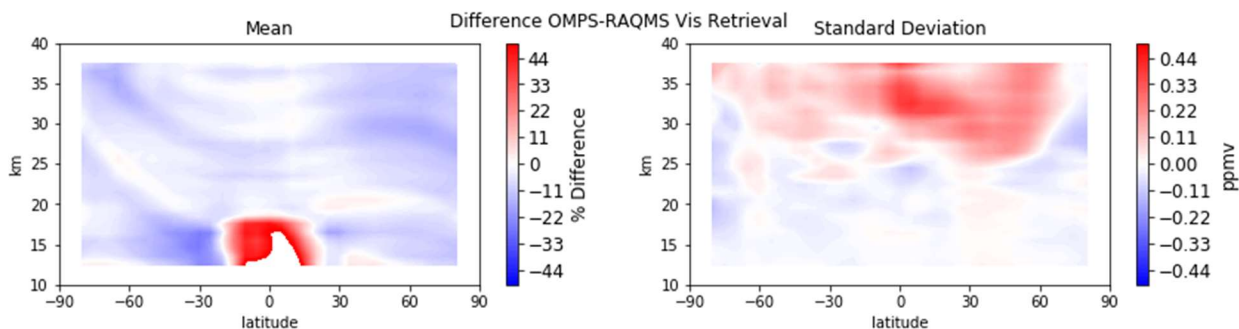


Figure 12. Difference in mean and standard deviation between OMPS-L visible retrievals and RAQMS-Aura.

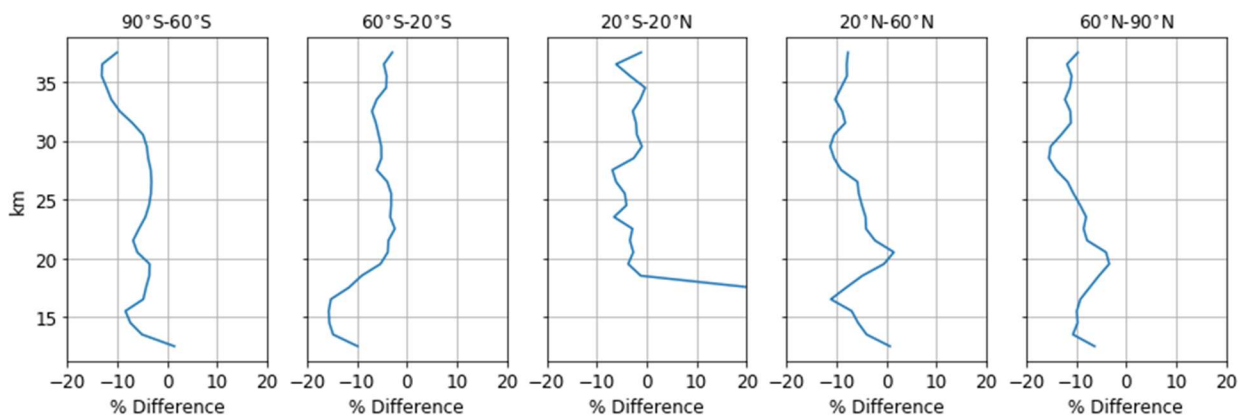


Figure 13. Regionally binned percent bias in OMPS-L visible retrievals for a) 90°-60° S; b) 60°-20° S; c) 20° S-20° N; d) 20°-60° N; e) 60°-90° N.

4.4.2 UV Retrieval

The 5° latitude bin-1 km altitude zonal mean percent difference is given in Fig.

14a. The zonal mean percent difference between the OMPS-L UV retrieval and corrected RAQMS-Aura is primarily slightly negative. The percent difference is within $\pm 10\%$ throughout nearly the entire domain, except above 50 km. Above 50 km is characterized by a large high bias.

Profiles of the percent difference between the OMPS-L UV retrievals and corrected RAQMS-Aura over the wide latitude bands is given in Fig. 15. The percent difference is largest above 50 km in all latitude bands. Between 30 km and 42 km for

90°-60° S, 60°-20° S, and 20°S-20°N OMPS-L is biased within $\pm 2.5\%$ of RAQMS-Aura. Between 42 km and 50 km for 90°-60° S and 60°-20° S, OMPS-L is biased -5-0% lower than RAQMS-Aura. Between 42 km and 50 km for 20° S-20°N, OMPS-L is biased between -10 and -2.5% lower than RAQMS-Aura. For the 20°-60° N and 60°-90° N latitude bands, below 35 km OMPS-L is biased -7.5-0% lower than RAQMS-Aura. Between 42 and 50 km in these bands OMPS-L is biased -10-0% lower than RAQMS-Aura. Between 35 and 42 km the bias in OMPS-L relative to RAQMS-Aura is negligible.

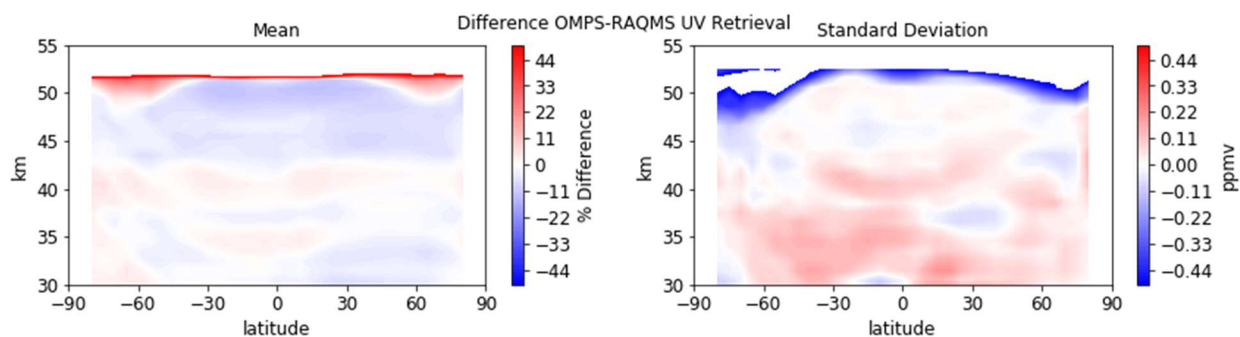


Figure 14. Differences for a) mean and b) standard deviation between OMPS-L UV retrievals and RAQMS-Aura retrievals.

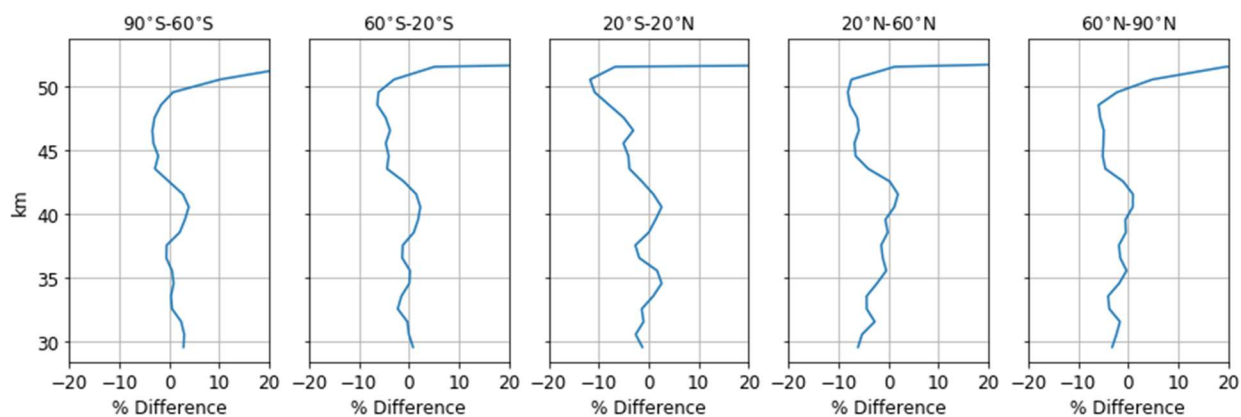


Figure 15. Regionally binned percent bias in OMPS-L UV retrievals for a) 90°-60° S; b) 60°-20° S; c) 20° S-20° N; d) 20°-60° N; e) 60°-90° N.

4.4.3 Overlap of UV and Visible Retrievals

The visible and UV retrievals overlap between 30.5 and 35.5 km. The percent bias between the UV and visible retrievals is displayed in Fig. 16. The UV retrieval is biased high for all altitudes and latitudes except for 30.5 km between the equator and 20° N. The bias between the two retrievals exceeds +10% between 90° and 60° S at 33.5 km, 34.5 km, and 35.5 km, between 70°S and 60°S at 31.5km and 32.5 km, and between 40°N and 80°N at 30.5 and 31.5 km. The bias for this region relative to RAQMS-Aura is generally lower for the UV retrieval than for the visible retrieval.

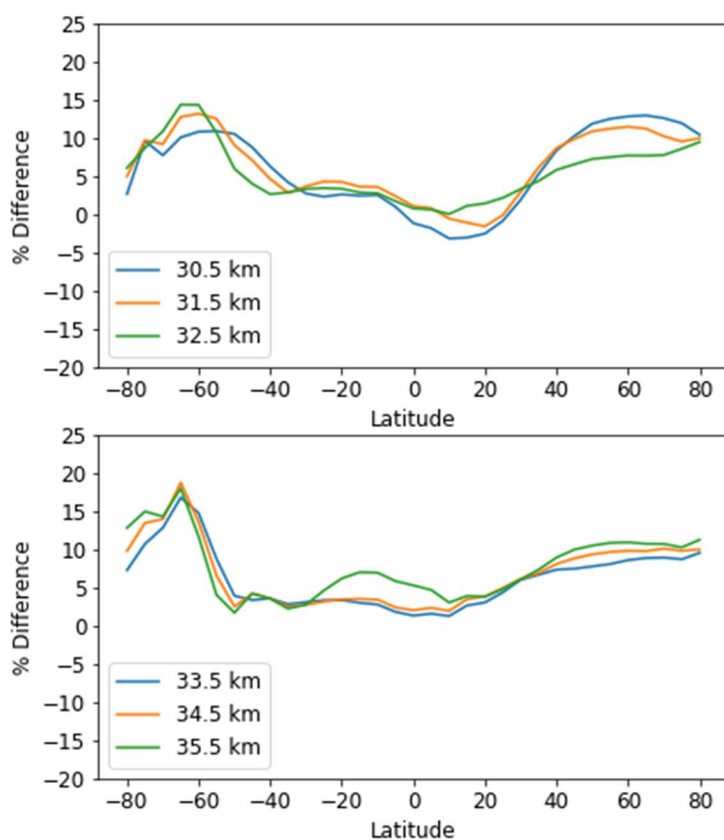


Figure 16. Percent difference between OMPS-L UV and visible retrievals at retrieval overlap altitudes of 30.5 km, 31.5 km, 32.5 km, 33.5 km, 34.5 km, and 35.5 km.

4.4.4 Seasonal Cycle in combined retrieval

As the calculated bias in the UV retrieval is less than that of the visible retrieval between 30 and 36 km, the Kramarova et al. 2018 method for combining the two retrievals into a single retrieved profile is applicable. This method uses the visible retrieval to 30.5 km and then the UV retrieval above 30.5 km. The seasonal cycle is calculated separately for OMPS-L and RAQMS-Aura as the percent deviation from the 2012-2016 mean concentration for the latitude and altitude, which can be reviewed in Fig. 2 and Fig. 5. Plots of the average annual cycle at 50°-55° S, 25°-30°S, and 65-70°N are displayed for consistency with Kramarova et al. 2018, but the cycle is calculated for all latitudes. The seasonal cycle for OMPS-L ppmv concentrations is shown in panel a of figures 17, 18, and 19. The seasonal cycle in RAQMS-Aura is shown in panel b of figures 17, 18, and 19. The difference in the seasonal cycle between OMPS-L and RAQMS-Aura is shown in panel c of figures 17, 18, and 19. In the difference calculation, a positive value indicates OMPS-L is higher than RAQMS-Aura and a negative value that OMPS-L is lower than RAQMS-Aura. Across all latitude regions, the average annual cycle below 50 km is similar for OMPS-L and RAQMS-Aura.

The annual cycle in the midlatitudes displays a seasonal shift in the comparative magnitude of the seasonal cycle for OMPS-L and RAQMS-Aura. In both hemispheres, the difference between the two cycles is positive in the spring/summer months and negative in the winter/fall months. The annual cycle is not constant with altitude, as for a given month the deviation from the zonal mean profile is positive at some altitudes and negative at others. The average annual cycle is similar for OMPS-L and RAQMS-Aura,

although the magnitude of the OMPS-L seasonal cycle is stronger below 40 km and weaker above 40 km than the magnitude of the RAQMS-Aura seasonal cycle.

The OMPS-L seasonal cycles presented in Figures 17a, 18a, and 19a are calculated from ozone concentration in ppmv, whereas Kramarova et al calculates seasonal cycle from ozone concentration in number density. This difference in how ozone concentration is expressed leads to a large apparent divergence between the two calculations of OMPS-L seasonal cycle in the midlatitudes above 20 km. For direct comparison of the OMPS-L seasonal cycle calculated by this study to the previous study, OMPS-L seasonal cycle is calculated from OMPS-L ozone concentrations expressed in number density. This new calculation of seasonal cycle for 50° - 55° S, 25° - 30° S, and 65° - 70° N is presented in Fig. 20 and compares favorably with the Kramarova et al seasonal cycles.

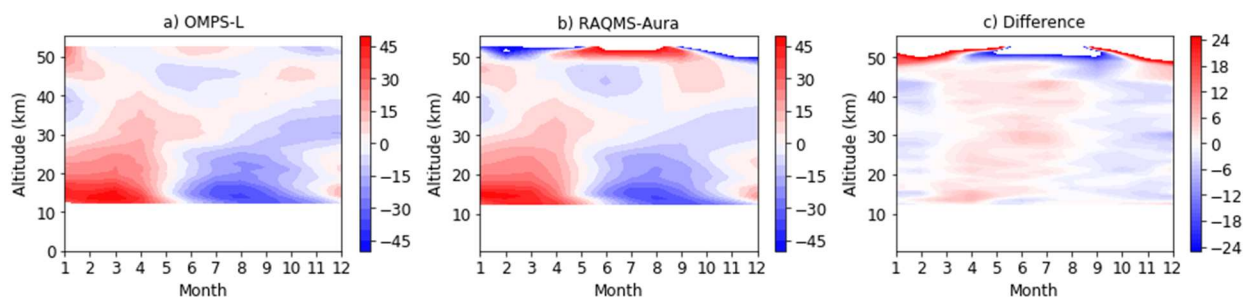


Figure 17. Average seasonal cycle at 65° - 70° N, expressed as a percent deviation from the mean for OMPS in ppmv.

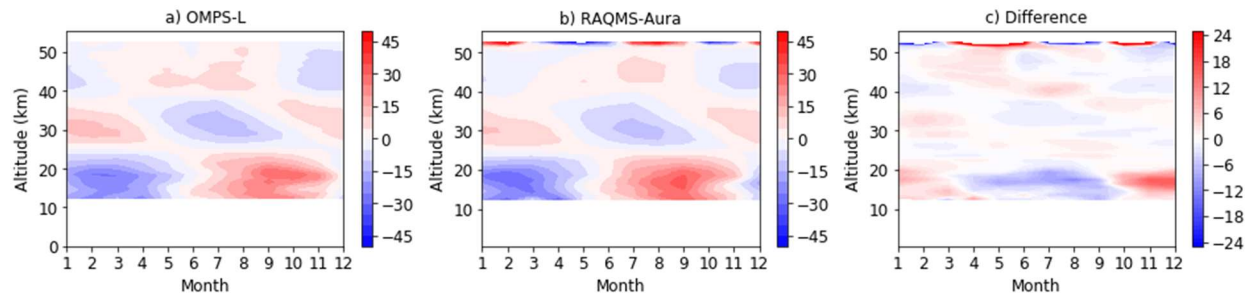


Figure 18. As in Fig. 17, except for the latitude band 25°-30°S.

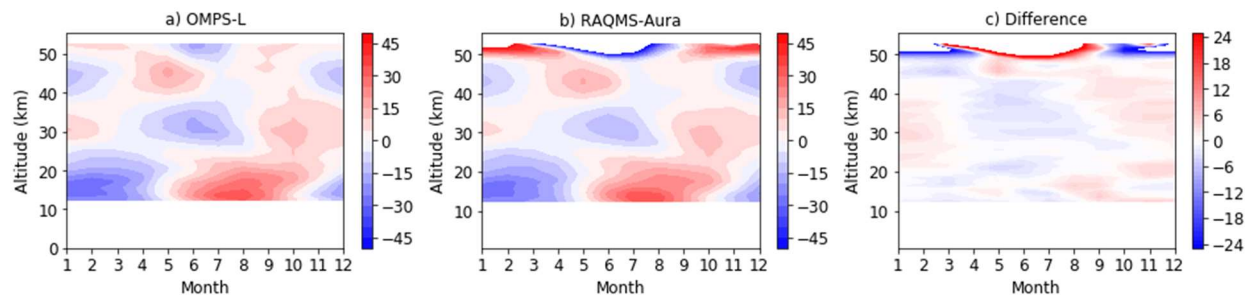


Figure 19. As in Fig. 17, except for the latitude band 50°-55°S.

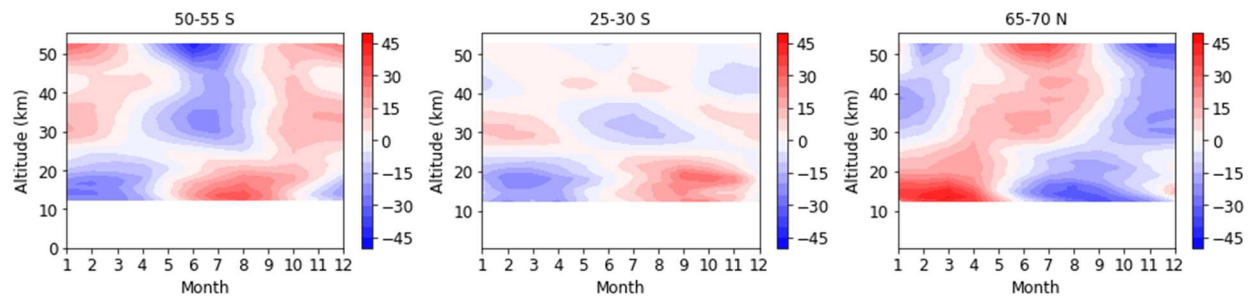


Figure 20. Seasonal cycle expressed as a percent deviation from mean for OMPS, and calculated from number density.

5. Conclusion

The RAQMS-Aura reanalysis is not a perfect representation of the atmospheric state, and at some locations and altitudes displays systematic biases when compared to ACE-FTS retrievals. Use of a zonal median difference from ACE-FTS retrievals as a correction factor brings RAQMS-Aura into average agreement with ESRL and SHADOZ ozonesonde measurements. RAQMS Aura is biased high compared to SHADOZ ozonesondes in the tropical troposphere, with a peak bias of 17% just above the tropopause. Based on this high bias in RAQMS-Aura relative to the SHADOZ ozonesondes, the high bias in tropical tropospheric ozone in OMPS-L is actually larger than calculated and the low bias in OMPS-L just above the tropical tropopause is closer to zero than calculated.

Excluding the tropical troposphere-lower stratosphere bias, OMPS-L visible retrievals are for the most part within $\pm 10\%$ of coincident RAQMS-Aura concentrations. Below 45 km, the OMPS-L UV retrieval is biased within approximately $\pm 5\%$ of coincident RAQMS-Aura concentrations. OMPS UV and Visible retrievals overlap in the region between 30 and 40 km, but the visible trends lower than the UV. This tendency in the overlap region and general trends in the bias agree with prior validation studies (eg. Kramarova et al. 2018). Excluding the tropical troposphere-lower stratosphere bias, OMPS-L ozone profile measurements are on average lower than RAQMS-Aura, ACE-FTS, and ozonesonde estimates of the true atmospheric ozone concentration. The average annual cycle is similar for OMPS-L and RAQMS-Aura, although the magnitude of the OMPS-L seasonal cycle is stronger below 40 km and weaker above 40 km than the magnitude of the RAQMS-Aura seasonal cycle.

The biases in OMPS-L calculated by this study provide observational error characteristics for assimilation of OMPS-L profiles into forecast models and analyses. This indirect validation of the OMPS-L ozone profiles shows that if assimilation were performed assuming OMPS-L measurements are unbiased or that the observation errors were lower than calculated here, the ozone analysis would tend to underestimate the actual ozone at altitudes where the retrieval is used to constrain the analysis. The produced analyses would be influenced by observation bias in addition to model bias, as would any calculations of trend or interannual variability in ozone using the produced analyses. To obtain ozone analyses which are reasonably representative of the true atmospheric ozone concentration, the bias in OMPS-L visible and UV retrievals must be accounted for in assimilation of the retrievals into atmospheric composition models such as RAQMS-Aura.

6. References

Analysis - AMS Glossary. (n.d.). Retrieved July 20, 2020, from

<http://glossary.ametsoc.org/wiki/Analysis>

Bai, K., Chang, N.-B., Shi, R., Yu, H., & Gao, W. (2017). An intercomparison of multidecadal observational and reanalysis data sets for global total ozone trends and variability analysis. *Journal of Geophysical Research: Atmospheres*, *122*(13), 7119–7139. <https://doi.org/10.1002/2016JD025835>

Bernath, P. F., McElroy, C. T., Abrams, M. C., Boone, C. D., Butler, M., Camy-Peyret, C., ... Zou, J. (2005a). Atmospheric Chemistry Experiment (ACE): Mission overview. *Geophysical Research Letters*, *32*(15), L15S01. <https://doi.org/10.1029/2005GL022386>

Bernath, P. F., McElroy, C. T., Abrams, M. C., Boone, C. D., Butler, M., Camy-Peyret, C., ... Zou, J. (2005b). Atmospheric Chemistry Experiment (ACE): Mission overview. *Geophysical Research Letters*, *32*(15), L15S01. <https://doi.org/10.1029/2005GL022386>

Bovensmann, H., Burrows, J. P., Buchwitz, M., Frerick, J., Noël, S., Rozanov, V. V., ... Goede, A. P. H. (1999). SCIAMACHY: Mission Objectives and Measurement Modes. *Journal of the Atmospheric Sciences*, *56*(2), 127–150. [https://doi.org/10.1175/1520-0469\(1999\)056<0127:SMOAMM>2.0.CO;2](https://doi.org/10.1175/1520-0469(1999)056<0127:SMOAMM>2.0.CO;2)

Burrows, J. P., Weber, M., Buchwitz, M., Rozanov, V., Ladstätter-Weißmayer, A., Richter, A., ... Perner, D. (1999). The Global Ozone Monitoring Experiment (GOME): Mission Concept and First Scientific Results. *Journal of the Atmospheric*

Sciences, 56(2), 151–175. [https://doi.org/10.1175/1520-0469\(1999\)056<0151:TGOMEG>2.0.CO;2](https://doi.org/10.1175/1520-0469(1999)056<0151:TGOMEG>2.0.CO;2)

Chapman, S. (1930). A Theory of Atmospheric Ozone. *Royal Meteorological Society Memoirs*. <https://doi.org/10.1002/qj.49705824304>

Considine, D. B., Natarajan, M., Fairlie, T. D., Lingenfelser, G. S., Pierce, R. B., Froidevaux, L., & Lambert, A. (2008). Noncoincident validation of Aura MLS observations using the Langley Research Center Lagrangian chemistry and transport model. *Journal of Geophysical Research*, 113(D16), D16S33. <https://doi.org/10.1029/2007JD008770>

Crutzen, P. J. (1988). Tropospheric Ozone: An Overview. In *Tropospheric Ozone* (pp. 3–32). Dordrecht: Springer Netherlands. https://doi.org/10.1007/978-94-009-2913-5_1

Danilin, M. Y., Ko, M. K. W., Froidevaux, L., Santee, M. L., Lyjak, L. V., Bevilacqua, R. M., ... Read, W. G. (2002). Trajectory hunting as an effective technique to validate multiplatform measurements: Analysis of the MLS, HALOE, SAGE-II, ILAS, and POAM-II data in October–November 1996. *Journal of Geophysical Research*, 107(D20), 4420. <https://doi.org/10.1029/2001JD002012>

de Laat, A. T. J., van Weele, M., & van der A, R. J. (2017). Onset of Stratospheric Ozone Recovery in the Antarctic Ozone Hole in Assimilated Daily Total Ozone Columns. *Journal of Geophysical Research: Atmospheres*, 122(21), 11,880–11,899. <https://doi.org/10.1002/2016JD025723>

Dupuy, E., Walker, K. A., Kar, J., Boone, C. D., McElroy, C. T., Bernath, P. F., ...

- Zawodny, J. M. (2009). *Validation of ozone measurements from the Atmospheric Chemistry Experiment (ACE)*. *Atmos. Chem. Phys* (Vol. 9). Retrieved from www.atmos-chem-phys.net/9/287/2009/www.atmos-chem-phys.net/9/287/2009/E.
- Fishman, J. (2003). *Handbook of Climate, Weather, and Water: Chemistry, Impacts and Applications*. T.D. Potter and B. Colman, editors. Wiley, New York.
- Flynn, L. E., Hornstein, J., & Hilsenrath, E. (2004). The ozone mapping and profiler suite (OMPS). In *IEEE International IEEE International IEEE International Geoscience and Remote Sensing Symposium, 2004. IGARSS '04. Proceedings. 2004* (Vol. 1, pp. 152–155). IEEE. <https://doi.org/10.1109/IGARSS.2004.1368968>
- Frederick, S. E., Cebula, R. P., & Heath, D. F. (1986). *Instrument Characterization for the Detection of Long-term Changes in Stratospheric Ozone: An Analysis of the SBUY/2 Radiometer*. *Journal of Atmospheric and Oceanic Technology* (Vol. 3). American Meteorological Society. [https://doi.org/10.1175/1520-0426\(1986\)003<0472:ICFTDO>2.0.CO;2](https://doi.org/10.1175/1520-0426(1986)003<0472:ICFTDO>2.0.CO;2)
- Froidevaux, L., Jiang, Y. B., Lambert, A., Livesey, N. J., Read, W. G., Waters, J. W., ... Wagner, P. A. (2008). Validation of Aura Microwave Limb Sounder stratospheric ozone measurements. *Journal of Geophysical Research*, *113*(D15), D15S20. <https://doi.org/10.1029/2007JD008771>
- Hassler, B., Daniel, J. S., Johnson, B. J., Solomon, S., & Oltmans, S. J. (2011). An assessment of changing ozone loss rates at South Pole: Twenty-five years of ozonesonde measurements. *Journal of Geophysical Research Atmospheres*, *116*(22),

1–12. <https://doi.org/10.1029/2011JD016353>

Heath, D. F., Krueger, A. J., Roeder, H. A., & Henderson, B. D. (1975). The Solar Backscatter Ultraviolet and Total Ozone Mapping Spectrometer (SBUV/TOMS) for NIMBUS G. *Optical Engineering*, *14*(4), 144323.

<https://doi.org/10.1117/12.7971839>

Heath, Donald F., Mateer, C. L., & Krueger, A. J. (1973). The Nimbus-4 Backscatter Ultraviolet (BUV) atmospheric ozone experiment — tow years' operation. *Pure and Applied Geophysics*, *106–108*(1), 1238–1253. <https://doi.org/10.1007/BF00881076>

Hilsenrath, E., Cebula, R. P., DeLand, M. T., Laamann, K., Taylor, S., Wellemeyer, C., & Bhartia, P. K. (1995). Calibration of the NOAA 11 solar backscatter ultraviolet (SBUV/2) ozone data set from 1989 to 1993 using in-flight calibration data and SSBUV. *Journal of Geophysical Research: Atmospheres*, *100*(D1), 1351–1366.

<https://doi.org/10.1029/94JD02611>

Holton, J. R., Haynes, P. H., McIntyre, M. E., Douglass, A. R., Rood, R. B., & Pfister, L. (1995). Stratosphere-troposphere exchange. *Reviews of Geophysics*, *33*(4), 403.

<https://doi.org/10.1029/95RG02097>

JACOB, D. J. (1999). Stratospheric Ozone. In *Introduction to Atmospheric Chemistry* (pp. 164–199). Princeton University Press. <https://doi.org/10.2307/j.ctt7t8hg.13>

Jaross, G., Bhartia, P. K., Chen, G., Kowitt, M., Haken, M., Chen, Z., ... Kelly, T. (2014). OMPS Limb Profiler instrument performance assessment. *Journal of Geophysical Research: Atmospheres*, *119*(7), 4399–4412.

<https://doi.org/10.1002/2013JD020482>

Jiang, Y. B., Froidevaux, L., Lambert, A., Livesey, N. J., Read, W. G., Waters, J. W., ...

Zablocki, G. (2007). Validation of Aura Microwave Limb Sounder Ozone by ozonesonde and lidar measurements. *Journal of Geophysical Research*, 112(D24),

D24S34. <https://doi.org/10.1029/2007JD008776>

Kramarova, N. A., Nash, E. R., Newman, P. A., Bhartia, P. K., McPeters, R. D., Rault, D.

F., ... Labow, G. J. (2014). Measuring the Antarctic ozone hole with the new ozone mapping and profiler suite (OMPS). *Atmospheric Chemistry and Physics*, 14(5),

2353–2361. <https://doi.org/10.5194/acp-14-2353-2014>

Kramarova, Natalya A., Bhartia, P. K., Jaross, G., Moy, L., Xu, P., Chen, Z., ... Sheese,

P. (2018). Validation of ozone profile retrievals derived from the OMPS LP

version 2.5 algorithm against correlative satellite measurements. *Atmospheric*

Measurement Techniques, 11(5), 2837–2861. [https://doi.org/10.5194/amt-11-2837-](https://doi.org/10.5194/amt-11-2837-2018)

2018

Lait, L. R., Newman, P. A., Schoeberl, M. R., Mcgee, T., Twigg, L., Browell, E. V., ...

Gerding, M. (2004). *Non-coincident inter-instrument comparisons of ozone measurements using quasi-conservative coordinates*. *Atmos. Chem. Phys* (Vol. 4).

Retrieved from www.atmos-chem-phys.org/acp/4/2345/

Levelt, P. F., van den Oord, G. H. J., Dobber, M. R., Malkki, A., Huib Visser, Johan de

Vries, ... Saari, H. (2006). The ozone monitoring instrument. *IEEE Transactions on Geoscience and Remote Sensing*, 44(5), 1093–1101.

<https://doi.org/10.1109/TGRS.2006.872333>

Loew, A., Bell, W., Brocca, L., Bulgin, C. E., Burdanowitz, J., Calbet, X., ... Verhoelst, T. (2017). Validation practices for satellite-based Earth observation data across communities. *Reviews of Geophysics*, *55*(3), 779–817.

<https://doi.org/10.1002/2017RG000562>

McPeters, R. D., Bhartia, P. K., Haffner, D., Labow, G. J., & Flynn, L. (2013). The version 8.6 SBUV ozone data record: An overview. *Journal of Geophysical Research: Atmospheres*, *118*(14), 8032–8039. <https://doi.org/10.1002/jgrd.50597>

Molina, M. J., & Rowland, F. S. (1974). Stratospheric sink for chlorofluoromethanes: Chlorine atom-catalysed destruction of ozone. *Nature*, *249*(5460), 810–812.

<https://doi.org/10.1038/249810a0>

Monks, P. S., Archibald, A. T., Colette, A., Cooper, O., Coyle, M., Derwent, R., ... Williams, M. L. (2015). Tropospheric ozone and its precursors from the urban to the global scale from air quality to short-lived climate forcer. *Atmos. Chem. Phys*, *15*, 8889–8973. <https://doi.org/10.5194/acp-15-8889-2015>

Morris, G. A., Gleason, J. F., Russell, J. M., Schoeberl, M. R., & McCormick, M. P. (2002). A comparison of HALOE V19 with SAGE II V6.00 ozone observations using trajectory mapping. *Journal of Geophysical Research*, *107*(D13), 4177. <https://doi.org/10.1029/2001JD000847>

Pierce, R. B., Schaack, T., Al-Saadi, J. A., Fairlie, T. D., Kittaka, C., Lingenfelter, G. S., ... Fishman, J. (2007). Chemical data assimilation estimates of continental U.S.

ozone and nitrogen budgets during the Intercontinental Chemical Transport Experiment-North America. *Journal of Geophysical Research Atmospheres*, 112(12). <https://doi.org/10.1029/2006JD007722>

Seftor, C. J., Jaross, G., Kowitt, M., Haken, M., Li, J., & Flynn, L. E. (2014). Postlaunch performance of the Suomi National Polar-orbiting Partnership Ozone Mapping and Profiler Suite (OMPS) nadir sensors. *Journal of Geophysical Research: Atmospheres*, 119(7), 4413–4428. <https://doi.org/10.1002/2013JD020472>

Sheese, P E, Boone, C. D., & Walker, K. A. (2015). Detecting physically unrealistic outliers in ACE-FTS atmospheric measurements. *Atmos. Meas. Tech*, 8, 741–750. <https://doi.org/10.5194/amt-8-741-2015>

Sheese, Patrick E, Walker, K. A., Boone, C. D., Bernath, P. F., Froidevaux, L., Funke, B., ... Von Clarmann, T. (2016). ACE-FTS ozone, water vapour, nitrous oxide, nitric acid, and carbon monoxide profile comparisons with MIPAS and MLS. <https://doi.org/10.1016/j.jqsrt.2016.06.026>

Smit, H. G. J., Straeter, W., Johnson, B. J., Oltmans, S. J., Davies, J., Tarasick, D. W., ... Posny, F. (2007). Assessment of the performance of ECC-ozonesondes under quasi-flight conditions in the environmental simulation chamber: Insights from the Juelich Ozone Sonde Intercomparison Experiment (JOSIE). *Journal of Geophysical Research*, 112(D19), D19306. <https://doi.org/10.1029/2006JD007308>

Sofieva, V. F., Kyrölä, E., Laine, M., Tamminen, J., Degenstein, D., Bourassa, A., ... Bhartia, P. K. (2017). Merged SAGE II, Ozone_cci and OMPS ozone profile dataset

and evaluation of ozone trends in the stratosphere. *Atmos. Chem. Phys.*, *17*, 12533–12552. <https://doi.org/10.5194/acp-17-12533-2017>

Solomon, S. (1999). Stratospheric ozone depletion: A review of concepts and history. *Reviews of Geophysics*, *37*(3), 275–316. <https://doi.org/10.1029/1999RG900008>

Solomon, Susan, Ivy, D. J., Kinnison, D., Mills, M. J., Neely, R. R., & Schmidt, A.

(2016). Emergence of healing in the Antarctic ozone layer. *Science*.

<https://doi.org/10.1126/science.aae0061>

Steinbrecht, W., Froidevaux, L., Fuller, R., Wang, R., Anderson, J., Roth, C., ...

Tummon, F. (2017). An update on ozone profile trends for the period 2000 to 2016.

Atmospheric Chemistry and Physics, *17*(17), 10675–10690.

<https://doi.org/10.5194/acp-17-10675-2017>

Stolarski, R. S., & Cicerone, R. J. (1974). *Stratospheric Chlorine: a Possible Sink for*

Ozone (Vol. 52). Retrieved from www.nrcresearchpress.com

Wargan, K., Labow, G., Frith, S., Pawson, S., Livesey, N., & Partyka, G. (2017).

Evaluation of the ozone fields in NASA's MERRA-2 reanalysis. *Journal of Climate*,

30(8), 2961–2988. <https://doi.org/10.1175/JCLI-D-16-0699.1>

Waters, J. W., Froidevaux, L., Harwood, R. S., Jarnot, R. F., Pickett, H. M., Read, W. G.,

... Walch, M. J. (2006). The Earth observing system microwave limb sounder (EOS

MLS) on the aura Satellite. *IEEE Transactions on Geoscience and Remote Sensing*,

44(5), 1075–1092. <https://doi.org/10.1109/TGRS.2006.873771>

- Waters, J. W., Read, W. G., Froidevaux, L., Jarnot, R. F., Cofield, R. E., Flower, D. A., ... Filipiak, M. J. (1999). The UARS and EOS Microwave Limb Sounder (MLS) Experiments. *Journal of the Atmospheric Sciences*, 56(2), 194–218.
[https://doi.org/10.1175/1520-0469\(1999\)056<0194:TUAEML>2.0.CO;2](https://doi.org/10.1175/1520-0469(1999)056<0194:TUAEML>2.0.CO;2)
- Waymark, C., Walker, K. A., Boone, C. D., & Bernath, P. F. (2013). ACE-FTS version 3.0 data set: validation and data processing update. *Fast Track-1*, 56.
<https://doi.org/10.4401/ag-6339>
- World Meteorological Organization. (1995). Scientific Assessment of Ozone Depletion: 1994.
- WMO (World Meteorological Organization), *Scientific Assessment of Ozone Depletion: 2018*, Global Ozone Research and Monitoring Project – Report No. 58, 588 pp., Geneva, Switzerland, 2018.
- Yumimoto, K., Tanaka, T. Y., Oshima, N., & Maki, T. (2017). JRAero: the Japanese Reanalysis for Aerosol v1.0. *Geoscientific Model Development*, 10(9), 3225–3253.
<https://doi.org/10.5194/gmd-10-3225-2017>
- Ziemke, J. R., & Chandra, S. (2012). Development of a climate record of tropospheric and stratospheric column ozone from satellite remote sensing: evidence of an early recovery of global stratospheric ozone. *Atmospheric Chemistry and Physics*, 12(13), 5737–5753. <https://doi.org/10.5194/acp-12-5737-2012>